Received: 1 August 2023 | Revised: 14 November 2023 | Accepted: 18 November 2023

DOI: 10.1111/ffe.14206

INVITED REVIEW

FFEMS Fatigue & Fracture of Engineering Materials & Structures WILEY

Fatigue limit estimation of metals based on the thermographic methods: A comprehensive review

Mohammad Zaeimi[1] | **Rosa De Finis**[2] | **Davide Palumbo**[1] | **Umberto Galietti**[1]

[1]Department of Mechanics, Mathematics and Management, Polytechnic University of Bari, Bari, Italy

[2]Department of Engineering for Innovation, University of Salento, Lecce, Italy

Correspondence
Umberto Galietti, Department of Mechanics, Mathematics and Management, Polytechnic University of Bari, Via Orabona, 70125 Bari, Italy.
Email: umberto.galietti@poliba.it

Funding information
European Union—NextGenerationEU, Grant/Award Number: CN00000023

Abstract

Infrared thermography has been under review in the last 30 years due to its versatility and potential in the detection of the thermal signature associated with intrinsic energy phenomena due to dissipative processes, specifically those relying on mechanical fatigue. Nowadays, it is a well-established technique that can support mechanical and structural engineers to implement a damage-tolerant design, assess the residual life, and finally characterize the fatigue behavior of materials. The aim of this work is to review all thermography-based approaches and procedures for fatigue limit estimation by rapid tests, drawing considerations on the applicability of thermal methods in fatigue assessment of mechanical components, proposing the capabilities of different thermal indices in fatigue assessment, and discussing the pros and cons of each method as well as the open points. On one hand, this review intends to sum up what has already been done in the field; on the other hand, it provides a guideline to direct new researches toward issues that should be resolved or understood.

KEYWORDS

fatigue assessments, NDT, rapid fatigue estimation, temperature evolution, thermographic method

1 | INTRODUCTION

Over the years, infrared (IR) thermography has proven to be a versatile tool in the field of experimental mechanics and mechanical design. This contactless and non-destructive technique allows for comprehensive structural integrity investigations[1,2] (the defect detection in steel plates,[3] composites,[4-7] 3D printed materials[8] and welded joints,[9] and the evaluation of fatigue cracks[10]), the stress analysis (thermoelastic stress analysis [TSA]) evaluations,[11-16] and energy-based assessments to study fatigue processes.[17,18]

Thermography-based methods have come a long way, thanks to improved equipment and robust data analysis tools. Nowadays, some considerations can be drawn upon the robustness and reliability of such methods to support fatigue investigations in terms of damage analysis and assessment, residual life predictions, and most importantly, fatigue limit estimations.[19,20]

Basically, the motivation for the development of alternative and innovative procedures to estimate the fatigue limit, relying on the use of an experimental technique during fatigue tests, can be attributed to two factors:

1. the rapidity of the testing procedures compared to classic protocols,
2. the potential to obtain more information about the material state during the loading.

Referring to the first point, classic and well-established fatigue characterization methods,[21,22] such as constant amplitude tests to obtain the Wöhler curve, serve as a standard approach. However, they are time and cost-consuming due to the number of samples being tested to obtain a statistically significant fatigue limit estimation, and the test duration involving high energy, operability, and maintenance costs. In general, a classic fatigue test involves a pristine material tested until the failure at a specific stress level, stress ratio, and mechanical frequency.

To reduce testing time and costs, rapid fatigue tests were developed according to the approach of La Rosa and Risitano.[22] This method entails using a series of constant amplitude loading blocks applied incrementally. During each block, the stress amplitude and mean stress increase while keeping the frequency and stress ratio constant for a specific number of cycles, continuing until material failure occurs. During such a test program, the material experiences different damage regimes,[23,24] as discussed later. The move from one regime to another results in shifts in behavior that can be associated with critical stages of fatigue life, leading to the fatigue limit estimation. In other words, the main concept behind the so-called "stepwise" test, is that the value of the fatigue limit coincides with the first significant temperature variation associated with the damage, using a specific loading procedure.[22-25]

Regarding the second point, a key role in the development of such a thermography-based technique is the possibility of obtaining more complementary information about the fatigue behavior, from a simple classic test. This includes the estimation of energy dissipated due to the fatigue and the identification of the onset and locations of damage.[26] The processing of thermal signal ensures somehow the just said outputs.

Indeed, it has been four decades since the development of tests using an IR camera to reliably capture parameters that describe fatigue processes.[27–31] The mentioned technique has undergone advancements in its original procedure and has seen numerous developments, especially in the evaluation of the heat sources related to intrinsic dissipations.[32,33] The approaches presented in the literature, relying on the estimation of heat sources accompanying damage phenomena,[31,34,35] are based on the assessment of specific energy-based indices/parameters, including

a. mean temperature increase (usually the mean value of the steady state temperature),[36-40]
b. initial slope of the temperature,[20,41,42]
c. energy loss per cycle,[43]
d. temperature harmonic components,[26,32,44,45]
e. loss of the adiabaticity which the approach relies on the study of the thermoelastic signal and the thermoelastic phase shift,[26,46-48] and
f. fracture fatigue entropy.[49]

Providing an overall perspective, Figure 1 highlights substantial progress in fatigue assessment through thermographic methods. It is worth noting that in addition to these advancements, further studies in this context will be discussed later.

In Figure 2, an overview of the main idea of the well-established methods based on the above parameters is presented. Once the parameters have been assessed, well-established procedures[21,22,50-52] can be applied to estimate the fatigue limit.

This study is organized as follows: In Section 2, the heat dissipations induced by fatigue damage are discussed. Section 3 covers the approaches relying on well-established methods to obtain thermal indices and recent advances. In Section 4, the basics of fatigue under stress-controlled tests and the typical experimental setups for fatigue tests using an IR camera are presented. Section 5 presents the procedures to obtain the fatigue limit using stepwise and static tensile tests, in a rapid way. Section 6 engages in a comprehensive discussion of the methods, highlighting their pros and cons, achieving milestones, and addressing open points for further improvement. Finally, Section 7 concludes the paper based on the findings presented.

2 | THEORY: HEAT SOURCES RELATED TO FATIGUE DAMAGE

2.1 | Micro/macro mechanisms involved in fatigue

As already demonstrated by pioneer researchers,[53] it is well-established that fatigue is a dissipative process[54-58] starting at the microscopic level[59-61] and culminating in fatigue cracks; as explained in the work of Schijve,[62] the crack onset occurs at stress amplitudes below the yield limit.

Bauschinger[60] showed that during cyclic loading, very small inelastic, that is, plastic, microstrains take place.[63] However, the microscopic reasons that cause fatigue failure remained unclear and were not thoroughly studied until the early twentieth century, when Ewing and Humfrey[64] observed the emergence of slip bands and microcracks on the surface of a fatigued steel. Later, the damage mechanics explained that the

FIGURE 1 Some milestones in developing the history of thermographic techniques for fatigue assessment. [Colour figure can be viewed at wileyonlinelibrary.com]

appearance of cyclic slips as a non-recoverable phenomenon due to strain hardening,[62] results in slip accumulation. This, in turn, leads to the formation of a microcrack, which has the potential to continue growing when subjected to additional cyclic loading, as illustrated in Figure 3A.

From a macroscopic point of view, the slip bands, produced during cyclic loading, result in the formation of

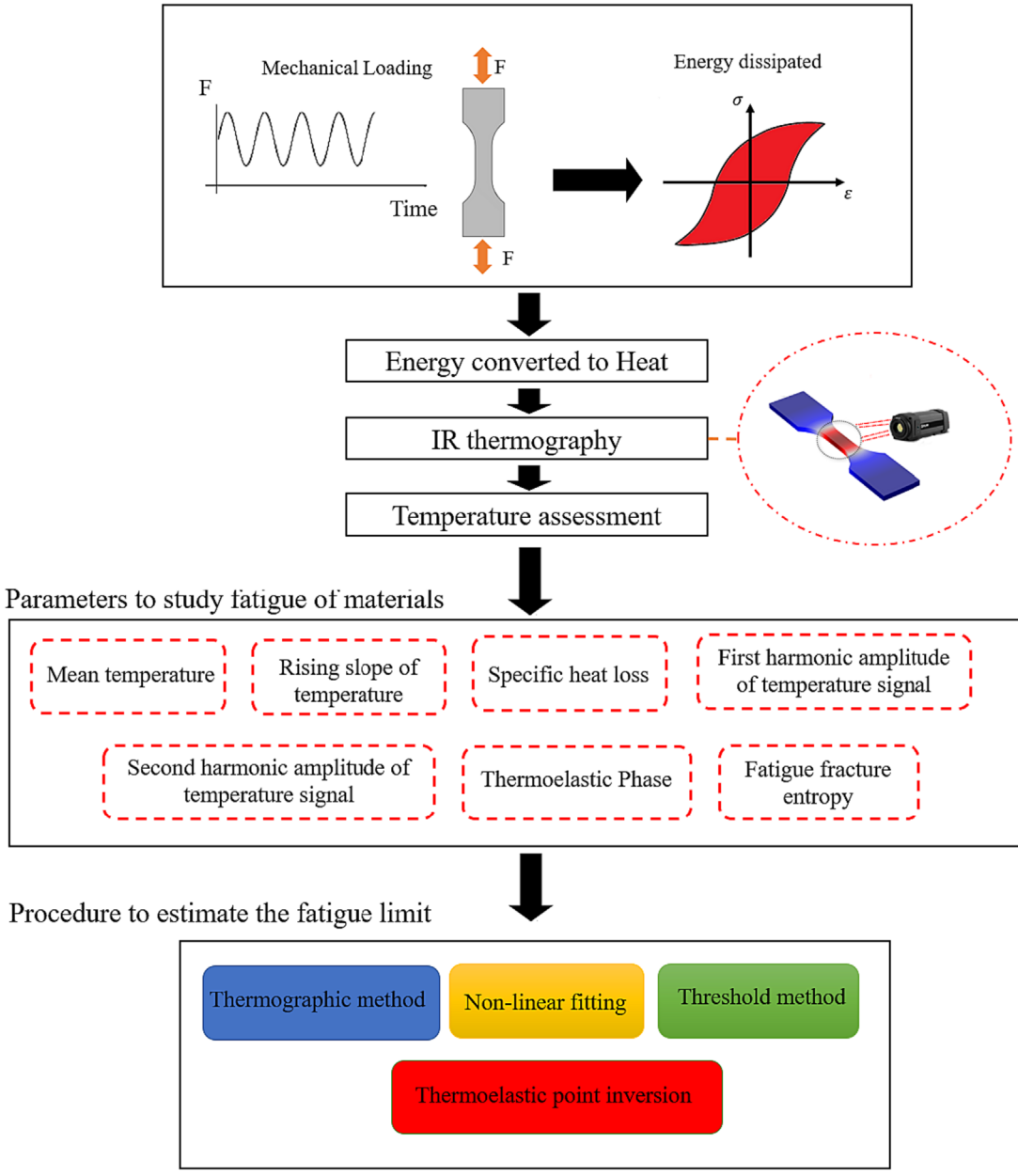

FIGURE 2 Thermal parameters to study fatigue and procedures for estimating fatigue limit. [Colour figure can be viewed at wileyonlinelibrary.com]

extrusion–intrusion pairs that in turn produce surface roughness; it could be a direct cause of crack initiation (see Figure 3).

According to Murakami,[63] the fatigue limit can be defined as the "threshold stress for crack propagation" rather than the "critical stress for crack initiation." The key, still relevant, conclusion drawn from the work of Bauschinger[60] and Ewing and Humfrey[64] is that fatigue damage results from the accumulation of many very small irreversible plastic cyclic microstrains.

2.2 | Energy dissipation in fatigue

Under an energetic point of view, during a fatigue test, by neglecting the possible phase transformations in material (i.e., shape memory alloys or crystallizable rubbers), two inner heat sources are generated due to mechanical loading: dissipative and thermoelastic sources.[67] The former contributes to the specimen's temperature increase, while the latter, the reversible one, is related to thermomechanical coupling phenomena. In Boulanger's work,[33]

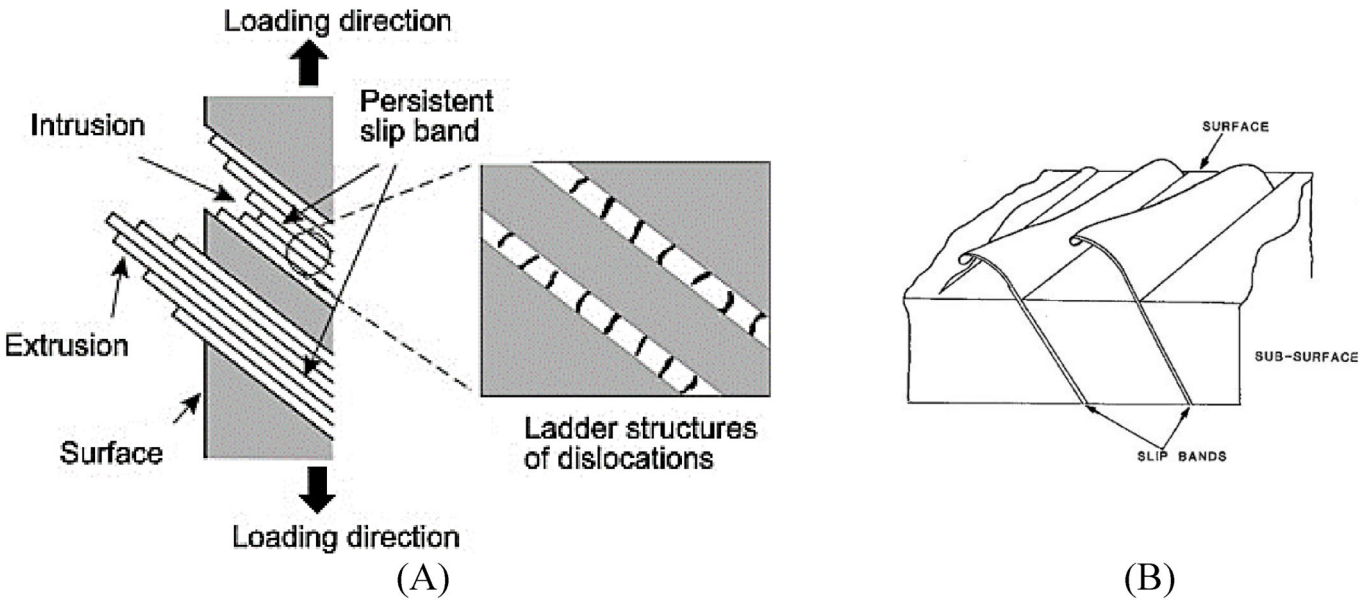

FIGURE 3 (A) Fatigue crack initiation mechanism[65] and (B) schematic illustration of slip band extrusions during a cyclic straining.[66]

the authors analytically separated the thermal contributions of the abovementioned sources to analyze their influence on fatigue damage, separately. Referring to the dissipative heat component, it is related to fatigue damage mechanisms due to the inelastic/anelastic behavior of the material.[61,68]

As discussed before, irreversible plastic deformations are responsible for crack nucleation/growth and propagation. When macroscopic strains are present in the material during fatigue tests, the mechanical energy is dissipated in each loading cycle. Graphically, this energy consumption can be represented by a hysteresis loop in the stress–strain curve[69-71] and the area is the measure of the dissipated energy. A portion of this energy converts into heating, while another portion remains internally stored, leading to irreversible deformations.[68,72,73]

As can be seen in Figure 4A, according to the first principle of thermodynamics applied to a body subjected to a mechanical load, the total power balance is as follows[72,73]:

$$\dot{W} + \dot{Q} = \dot{U} = \dot{E}_{rev} + \dot{E}_d + \dot{E}_s, \tag{1}$$

where $\dot{W}$ is the rate of total work energy supplied to the material, $\dot{Q}$ is the rate of the heat exchanged with the environment, and $\dot{U}$ is the internal energy variation from the initial to the end of the test. $\dot{E}_{rev}$ is the power of reversible energy variations, $\dot{E}_d$ is the portion of supplied mechanical power that converts into heating, and $\dot{E}_s$ is the rate of internal energy that does not convert into

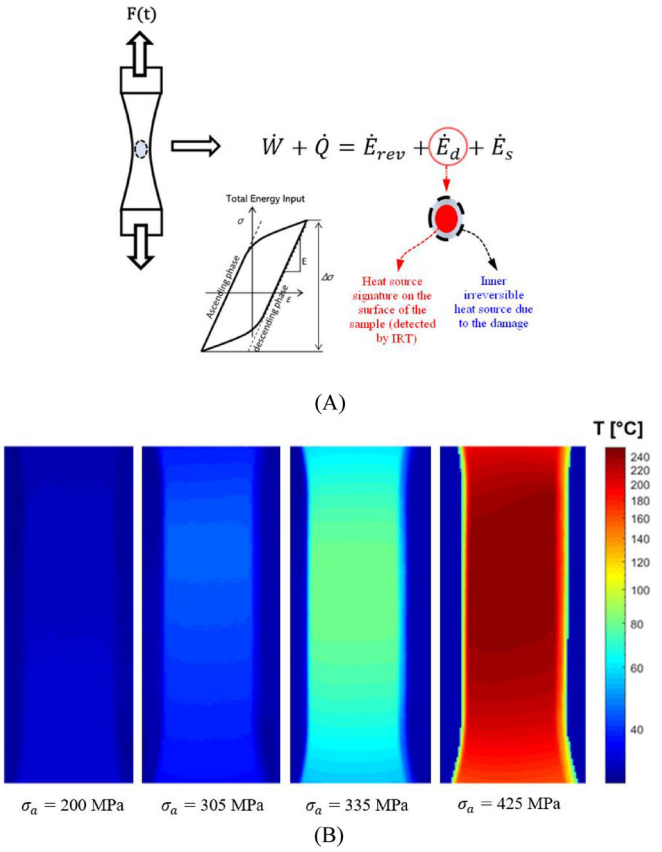

FIGURE 4 (A) Energy balance during cyclic loading.[72] (B) The temperature change during the fatigue test for the C45 specimen tested at $R = -1$ ($\sigma_a = 200$ MPa and 305 MPa below the fatigue limit, $\sigma_a = 335$ MPa above the fatigue limit, and $\sigma_a = 425$ MPa at the end of the test).[74] [Colour figure can be viewed at wileyonlinelibrary.com]

heating. The combination of $\dot{E}_d + \dot{E}_s$ represents the rate of irreversible energy variations that are related to fatigue damage. Different techniques indirectly derived it by analyzing the difference between the mechanical energy $(\dot{W})$ and the energy released as heat $(\dot{Q})$.[73] It should be noted that an inner heat source due to the damage (the blue circle in Figure 4A), produced during the cyclic loading, can be detected by its signature on the surface of the specimen (the red circle in Figure 4A) using the Infrared thermography technique. For instance, in Figure 4B, a temperature map associated with a C45 specimen subjected to fully reversed loading ($R = -1$) can be observed. These maps illustrate how temperature changes at the specimen's surface, acting as an indicator of dissipation, in response to the stress amplitude. Below the fatigue limit, this temperature increase is minimal. However, beyond the fatigue limit, it rises significantly as damage accumulates, ultimately reaching its highest point when the specimen fails.

2.3 | The relationship between energy dissipation and temperature

Stress–strain hysteresis behavior in metals is dependent on micromechanisms, which dissipate energy during cyclic deformation. These processes determine a loss of linearity between the applied stress and the corresponding strain leading to a lag in the response of the material (strain) to the applied stress[70] and ultimately the appearance of the hysteresis loop (from Greek ὑστέρησις = hysteresis = delay). The ability of materials to dispel energy by internal adjustments is referred to as damping.[71]

In general, when a material undergoes cyclic loading, it generates heat. This heat dissipation is a result of the material's internal friction and damping. The total energy dissipated by this internal friction during cyclic loading is the sum of all the individual work done within the various elements of the material. Considering sinusoidal stress applied to the material and due to the imperfect elasticity of the material, the unit deformation will not be equal instant by instant to the ratio of stress to the modulus of elasticity (σ/E), as predicted by elastic theory. Instead, it will intermittently deviate from this theoretical value. This leads to the stress–strain diagram taking the form of a closed curve known as a "hysteresis loop." The area enclosed by this loop represents the energy dissipated by internal damping within a unit volume during a single cycle.[75,76]

As the temperature is a sentinel of inner heat sources produced by cyclic loading, different authors studied the thermal signature associated with reversible and irreversible heat sources[12,13,18,46,72,77,78] as shown in Figure 5. In this figure, the quantities $\Delta\theta_E$ and $\Delta\theta_D$ are respectively the phase lags due to thermal diffusion of the first harmonic and second harmonic and $\Delta\theta$ the difference between them.

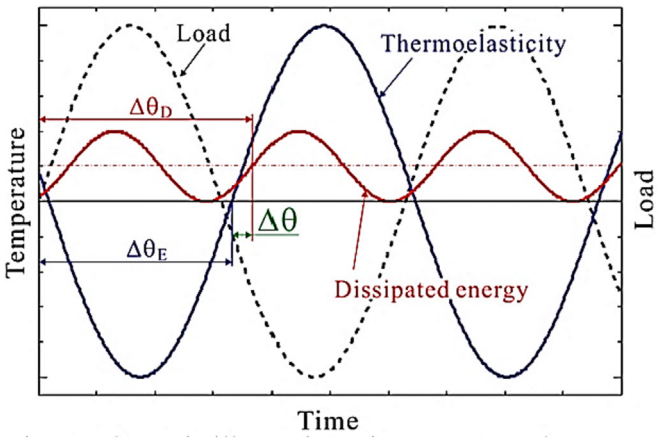

FIGURE 5 Schematic illustration of temperature variations due to reversible (thermoelastic) and irreversible (dissipated energy) phenomena.[32] [Colour figure can be viewed at wileyonlinelibrary.com]

The reversible energy variations produced by small volume changes inducing the "thermoelastic effect"[26] are represented in Figure 6. In the case of uniaxial sinusoidal loading, the thermoelastic coupling-related temperature variations can be expressed as follows:

$$T = T_{the} \sin(2\pi ft + \pi + \varphi), \tag{2}$$

where T is the temperature variations at the mechanical exciting frequency f, T_{the} is the peak-to-peak signal amplitude, and φ is the phase angle between temperature and loading signal.[79] According to the classic theory of thermoelastic stress analysis, the temperature and first stress invariant have opposite signs,[13] which is why "π" is included in Equation (2). Figure 6 depicts the relations between T and φ in two opposite cases.[26,47]

A phase shift depending on several factors can occur in the presence of phenomena leading to the loss of adiabatic conditions. The loss of adiabaticity can be associated with a thermal dissipative process.

In general, intrinsic dissipations produce heating in the form of two distinct contributions:

- the heat produced under the hysteresis conditions (anelastic regime),[61]
- the heat produced under visco-plastic deformations regime,[58,80]

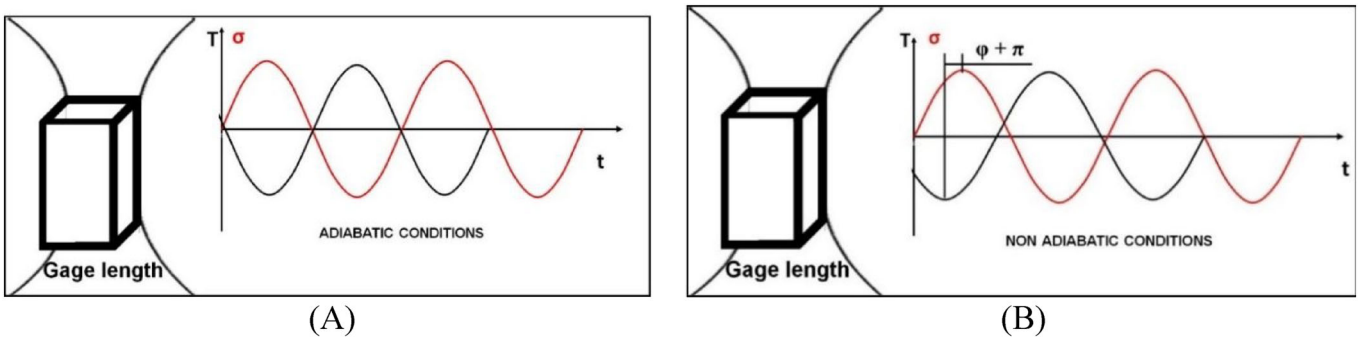

FIGURE 6 Thermoelastic phase shift φ: temperature and stress relation (A) under adiabatic conditions and (B) under non-adiabatic conditions.[26] [Colour figure can be viewed at wileyonlinelibrary.com]

These heat contributions, clearly affect the adiabaticity of the processes and then determine the variation in φ values. It is necessary to remark that in the case of a purely elastic cyclic response, the adiabaticity level (and the value of φ) depends on the loading frequency. The higher the loading frequency, the higher the adiabaticity level.

By focusing on the irreversible energy variations during fatigue tests (Figure 4A), the irreversible work energy supplied to the material depends on the adopted stress ratio. When the stored energy E_s is negligible, heat-converted energy (E_d) can be obtained directly from thermodynamic balance. E_d, however, can be assessed by analyzing the surface temperature of the sample[6,81] and can be expressed as follows:

$$E_d = \rho\, C_p \Delta T_d, \tag{3}$$

where ΔT_d are the dissipative temperature variations, ρ is the density, and C_p is the heat capacity at constant pressure. In previous research, Jordan[30] found a direct relationship between the mechanical energy variation (area under the hysteresis loop) and heat-converted energy during fatigue. Figure 7A shows the variation of the hysteresis loop within the fatigue regimes during classic constant amplitude tests to build Wholer's curve.[68]

2.4 | Self-heating effect

During rapid fatigue tests,[82] a self-heating effect (the mean steady-state temperature variations with the stress amplitude)[35,83] is produced in the material involving two mechanisms. According to Mareau,[83] the first one is associated with a reversible movement of the dislocations (mechanically reversible but thermally irreversible) and the second one is with plastic activity. The latter is associated with the progressive appearance of microplasticity,[84] while some open points still exist about the mechanisms occurring during the primary regime.

In Figure 7B, according to Munier's study,[35] a model was proposed to link the self-heating measurements and high cycle fatigue properties of metals in terms of temperature variations. In particular, in Figure 7B a representative elementary volume (REV) is defined as an elasto-plastic matrix containing several lattice discontinuities e.g. inclusions.

At low stress amplitudes, inclusions were considered to behave in the same way as the matrix, while the dissipation was mainly due to the elasto-plastic behavior of the matrix. However, once the stress exceeded a certain threshold, plastic hardening within the inclusions became active. In these conditions, the dissipation associated with the matrix corresponds to the primary regime, while the dissipation in the set of inclusions was linked to the secondary regime. The latter, according to Munier's approach,[35] governed the physical process of fatigue damage initiation.

In the following sections, the well-established and recent advanced approaches to obtain thermal parameters to study fatigue behavior are presented.

3 | DIFFERENT METHODS TO INVESTIGATE THE THERMAL BEHAVIOR FOR FATIGUE PREDICTION

3.1 | Direct temperature assessment

3.1.1 | Mean temperature increase

The self-heating phenomenon can be traced back to the work by Stromeyer[85] in 1914. Since then, it has been used for rapid fatigue limit prediction. In 1983, the pioneer researcher, Risitano,[23] and in 1986 Curti et al,[86] explored

the ability of thermography as a non-contact sensing technique for determining the fatigue limit based on the surface temperature.[22]

It is worth noting that the variation in the surface temperature is mainly due to a macroscopic result of the energy transfer. The advent of heat dissipation and self-heating regime during the cyclic loading can be mainly tracked by internal mechanisms of fatigue damage or simply microplasticity. Furthermore, external factors, for example, thermal convection and radiation, can significantly affect the temperature change.[40,74,77]

La Rosa and Risitano[22] studied the behavior of the surface temperature of specimens under cyclic loading. As proposed in Figure 8, (N_s and N_f are the number of cycles to reach the stabilized temperature and the failure, respectively), for loads higher than the fatigue limit, the temperature exhibits a typical behavior. It shows an increase from the beginning of the test (Phase 1), followed by a "stabilization" stage (Phase 2) until a short time before failure, and finally a sharp increase before the failure (Phase 3).

They noted that the greater the stress with respect to the fatigue limit, the higher the rate of temperature in Phase 1 and the "stabilization" temperature in Phase 2.[22,24] By using the temperature of the steady state (ΔT_{steady}) acquired during a stepwise loading procedure, it is possible to investigate the fatigue behavior of material and components.[25,26]

In another pioneer study,[21] intrinsic dissipation was introduced by Luong as an accurate indicator of damage

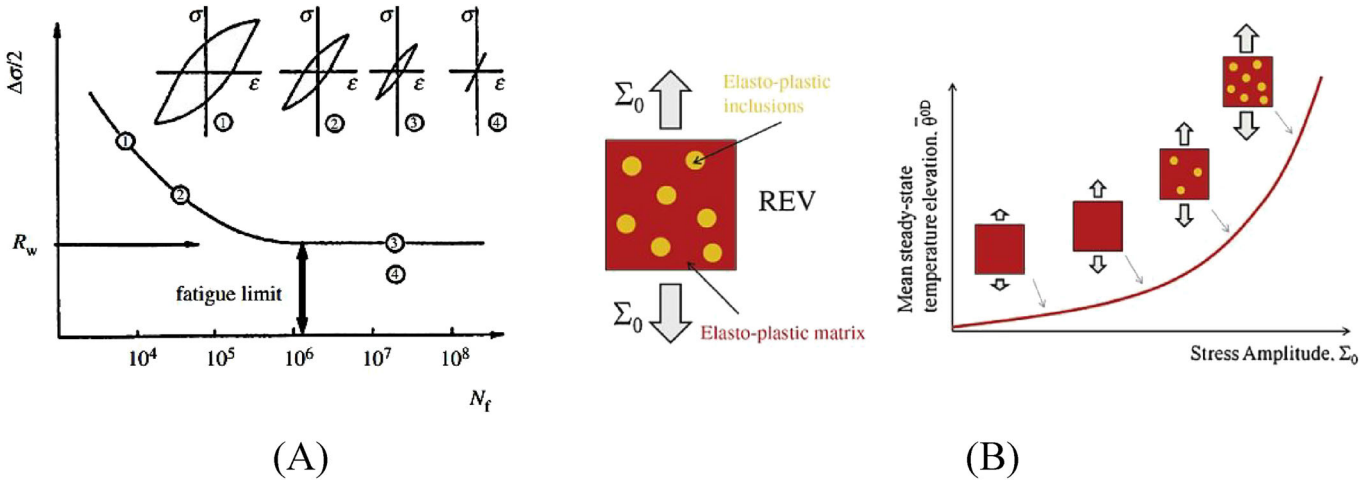

FIGURE 7 (A) Fatigue life and dissipated energy.[68] (B) Modeling of men temperature variations and micromechanical damage processes.[35] [Colour figure can be viewed at wileyonlinelibrary.com]

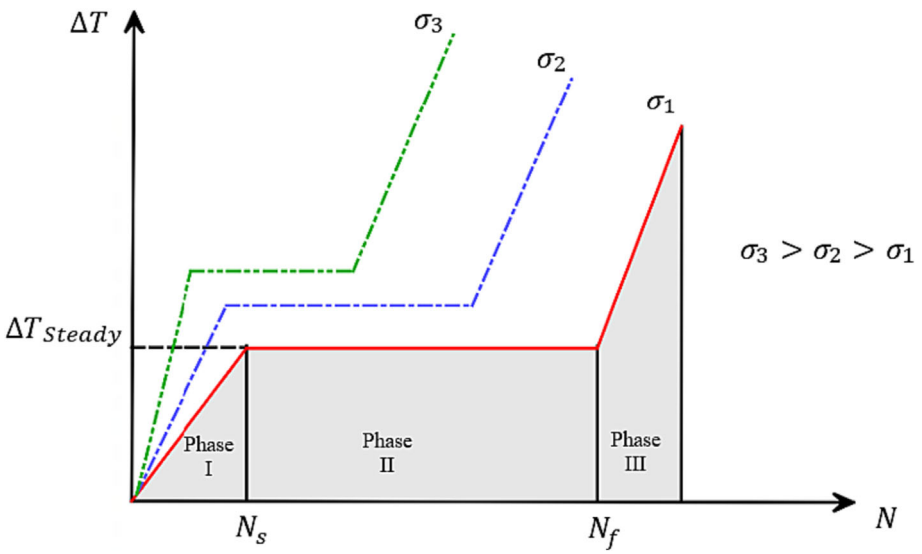

FIGURE 8 Surface temperature behavior and phases (thermal increments vs. the number of cycles). [Colour figure can be viewed at wileyonlinelibrary.com]

initiation. Using the coupled thermomechanical equation and subtracting the thermal image at different reference times, it became possible to estimate intrinsic dissipation based on the mean temperature.

It should be noted that the quantification of the intrinsic dissipation for engineering materials poses some challenges. For example, the measurements of surface thermal signature can be affected by heat exchanges, making the resulting measurement merely an estimate of the internal energy dissipated.[25] The quantification of intrinsic dissipation becomes more complex when dealing with brittle or highly diffusive materials due to small temperature changes,[25] which requires the development of specific smoothing procedures. For this purpose, De Finis et al,[25] developed a new procedure of thermal data analysis. They filtered out the superficial temperatures including the environmental temperature and the one produced by the heating from the hot servo-hydraulic fixture of the loading machine. On one hand, the ambient temperature effect was removed by subtracting the surface temperature of a dummy specimen from the surface temperature of the sample. On the other hand, the loading machine contribution was eliminated by assuming a linear temperature increase and using a specific data fitting procedure for thermal profiles in the longitudinal direction of the gage length. These recent advances in image processing, have enhanced the capability of IR thermography to detect the fatigue limit for different types of materials, particularly automotive components, and stress paths (reversed tension, rotating bending, cyclic torsion, etc.).[81]

As shown in Figure 9, the onset of the evolution of damage and defects leads to changes in the dynamic characteristics. Specifically, it affects properties such as the specific damping capacity Ψ, and the natural frequency of the materials which are related to damping parameters (e.g., the loss factor and damping ratio).[78] Damping is a material or system property to dissipate energy under cyclic loading, which can be obtained either from the exponential free decay curve or the half-power bandwidth method in the time or frequency domain, correspondingly.[78] Crupi found a relationship between the stabilized temperature increment, $\Delta T_{\text{stabilized}}$, and the square of the applied stress amplitude (σ_a^2) based on damping parameters as follows[78]:

$$\begin{cases} \Delta T_{stabilized} = 0, & \sigma_a < \sigma_c \\ \Delta T_{stabilized} = a\,\sigma_a^2 + b, & \sigma_c \le \sigma_a \le \sigma_y \end{cases} \tag{4}$$

where a and b denote material constants depending on the specific damping capacity Ψ and σ_c and σ_y are the fatigue limit and the stress amplitude, respectively.

The specific damping capacity is related to the stabilized hysteresis loop, a fatigue parameter, and $\Delta T_{\text{stabilized}}$. Briefly, $\Delta T_{\text{stabilized}}$ related to different loading levels can be found by acquiring thermal sequences in a stepwise loading of a single specimen.[78] It is worth noting that other relations as the same as the above power function can also be found in the literature but with different exponents.[22,87-90]

The relationship between $\Delta T_{\text{stabilized}}$ and σ_a was further developed by considering the number of cycles to the failure (N_f). Using the shakedown theory and multiscale concept, Wang et al[91] provided theoretical support for the relevant energy analysis and an intrinsic correlation between the above three parameters and called it quantitative thermographic methodology (QTM).

Recently, Feng et al[92] proposed a modified version of QTM by including the heat exchange with the help of the heat diffusion equation[18,33] and considering the variable amplitude loading. They assumed that the damage could

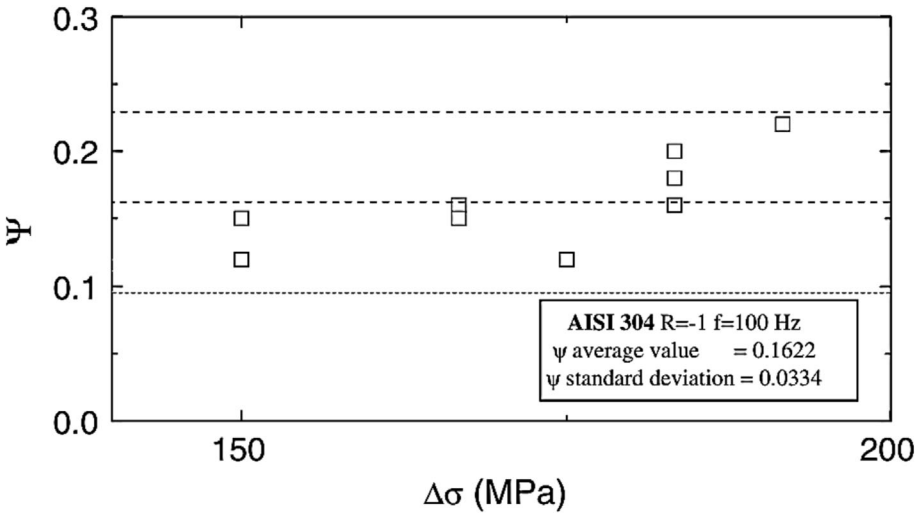

FIGURE 9 Specific damping Ψ versus the stress range $\Delta\sigma$, relative to AISI304 specimens at a load ratio $R = 1$ and a frequency $f = 100$ Hz.[78]

be equivalently transformed from one loading block to another.[93]

3.1.2 | Initial slope of the temperature curve

Through the fatigue tests, it was shown that there exists a close connection between the temperature rise and the material degradation under cyclic load. For aluminum 6061-T6, Figure 10 shows the evolution of the temperature slope as a function of the normalized number of cycles with respect to the number of cycles to failure. It can be seen that it increases at the beginning of the test, followed by a rapid decline, and then remains relatively flat in the stabilization phase for about 90% of the lifespan before rising sharply at the end.[82]

As a pioneer, Huang et al[94] experimentally observed a sharp increase in temperature, for some stainless steel and superalloys, shortly after reaching a steady-state condition. This temperature increase, as shown in Figure 11, was linked to the commencement and spread of macrocracks [50] and the forthcoming fracture.[37] However, this temperature rise seems to be an ineffective index since it is determined after a huge damage accumulation and involves a time-consuming process.

On the other hand, on the left-hand side of the temperature curve in phase I before the stabilization, the temperature rise angle was reported to be a possible index for fatigue assessment, as already mentioned in pioneer works by Curti et al[86] and Botny and Kaleta.[95] Boulanger et al,[33] showed that the initial slope of the temperature rise was useful for studying the fatigue behavior and specifically for estimating the dissipated energy. Mehdizadeh and Khonsari[49] proposed that the capability of this slope (see Figure 12A) for fatigue limit estimation depends on the sharp slope change in $R_\theta - \sigma$ curve (see Figure 12B for SS 304 with fatigue limit around 230 MPa[49]). In addition, a relation for determining the fatigue life as a function of the temperature slope in the first phase of the temperature trend was reported by Amiri and Khonsari.[41,42]

Since the slope of the temperature evolution, $R = \Delta T/N$, is measured in the early stages of the test, it offers a very rapid technique to predict fatigue life, preserving testing time and avoiding catastrophic failure. However, the drawback is that the relationship applies specifically to fatigue tests conducted on pristine

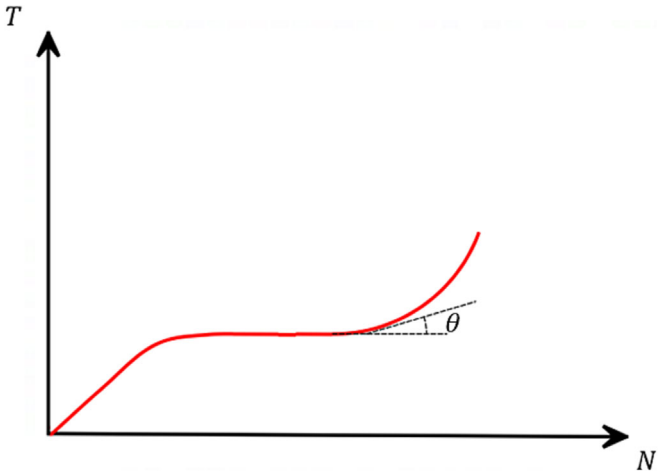

FIGURE 11 Temperature slope just after a steady-state condition. [Colour figure can be viewed at wileyonlinelibrary.com]

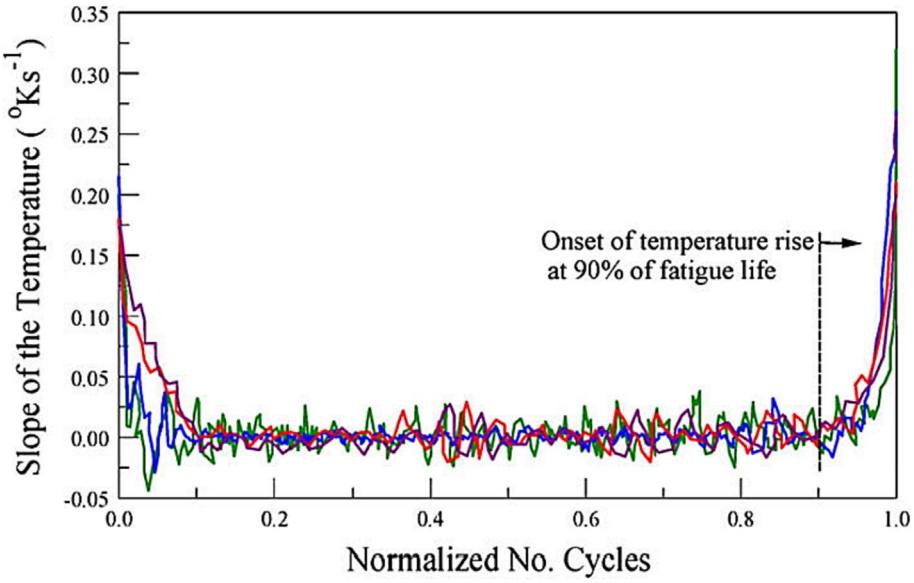

FIGURE 10 The evolution of the temperature slope in bending fatigue of aluminum 6061-T6.82 [Colour figure can be viewed at wileyonlinelibrary.com]

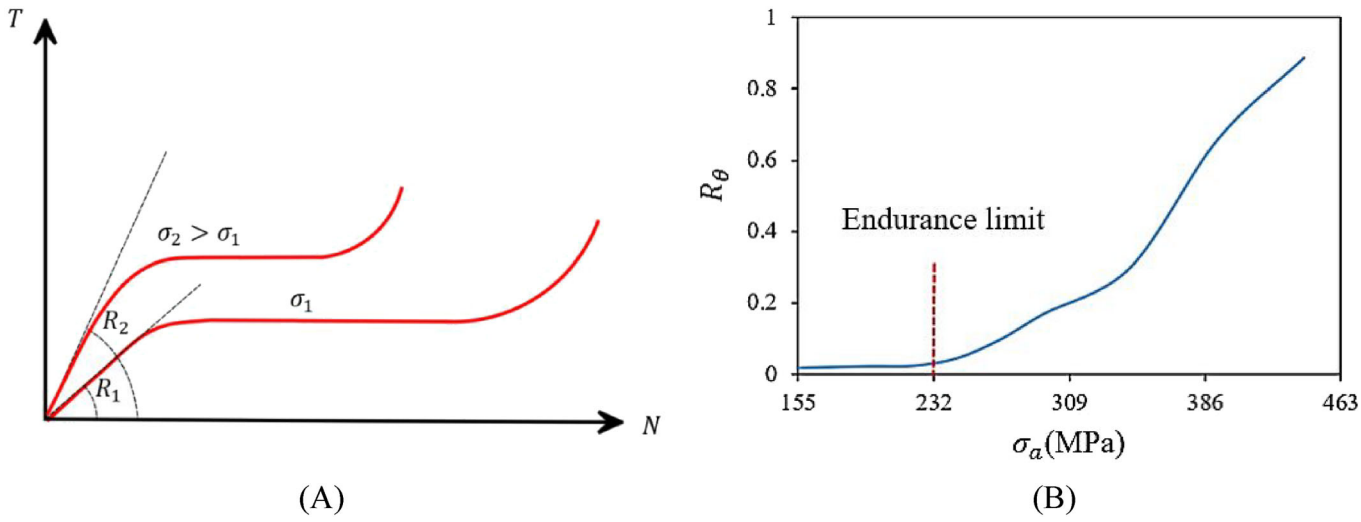

FIGURE 12 (A) Temperature slope at the beginning of the test and (B) fatigue limit predicted by initial slope of temperature for SS 304 (redrawn based on Amiri and Khonsari[41]). [Colour figure can be viewed at wileyonlinelibrary.com]

specimens without any prior damage. In other words, it does not account for the history of the specimen. Meyendorf et al[96] demonstrated that when the specimen has already experienced fatigue, its microstructure has been changed and thus its thermal response differs from the pristine specimen. Through a series of fatigue tests on cylindrical dog-bone samples machined from forged titanium, they reported a gradual change in the rate of temperature as the number of cycles accumulated.[96] To eliminate this limit, Khonsari and colleagues modified the aforementioned relationship by considering the accumulated damage for a non-pristine sample.[20]

As the sample experiences cyclic fatigue, the temperature rises after each step considerably increases. According to this observation, Amiri and Khonsari[20] proposed that this slope as a function of time can be utilized to estimate the remaining This approach allows for the quantification of prior fatigue damage. It is worth pointing out that all of these works were accomplished during an excitation loading, which involves a short-time mechanical loading.[96]

In another work by Liakat and Khonsari,[97] the relative slope (R_r) was introduced for predicting the remaining fatigue life. It was defined as a difference between the slope of the temperature rise (R) and the intercept of the slope and number of load cycles (R–N) curve. By defining the relative slope R_r, Liakat and Khonsari[97] showed that it exhibits a linear function of N and can be applicable to both constant and variable amplitude cyclic loadings. Furthermore, the slope of temperature can be utilized to predict fatigue life by estimating the entropy accumulation and plastic energy generation,[98] which are discussed later.

3.2 | Thermoelastic stress analysis

Although the thermoelastic effect was observed by Gough,[36] the first experiments were performed by Weber,[99] and eventually, the theoretical foundations were defined by Thomson (later known as Lord Kelvin).[100] Briefly, the concept of thermoelastic stress analysis (TSA) is based on the reversible temperature changes during the elastic deformation of a homogenous solid under adiabatic conditions. Under these assumptions, a linear relationship between surface temperature variations and the first invariant of stress can be defined[15,16,101-103] considering the classic TSA equation[103]:

$$\rho C_p \frac{\Delta T}{T_0} = -\alpha \Delta s, \tag{5}$$

where ρ is the density, C_p is the specific heat under constant strain, ΔT is temperature change, T_0 is the reference temperature, α is the coefficient of linear thermal expansion, and Δs is the change of the first invariant of the stress tensor.[102] This linearity is violated in the presence of non-adiabatic phenomena like heat diffusion due to the intrinsic damage. A detailed review of this can be found in the studies conducted by Wong et al.[102,104,105]

In the classic TSA equation, the temperature variations can be described as follows by considering uniaxial stresses with sinusoidal loading:

$$T = \frac{\alpha}{\rho C_p} T_a \sin(\omega t + \pi + \varphi). \quad (6)$$

Equation (6) presents a phase angle between temperature and loading signal, which depends on different factors such as the thickness of the painting or the gripers. When high-stress gradient and viscoelastic–plastic behavior are present, notable changes occur in the phase signal due to the departure from adiabatic conditions and the emergence of fatigue damage.[47]

As mentioned before, the capability of TSA is not limited to the presence of the adiabatic condition. Thermoelastic temperature amplitude ($T_{1\omega}$) and thermoelastic phase can be used as indicators of non-adiabatic condition, indirectly leading to the study of damage behavior of material estimating the fatigue limit during a stepwise loading test,[30,44,45,106,107] as presented below.

3.2.1 | Loss of adiabaticity (thermoelastic phase analysis)

Palumbo and Galietti[47] proposed a novel empirical method to study the fatigue behavior of stainless steels, called thermoelastic phase analysis (TPA), based on the phase of the thermoelastic signal. In addition, TPA can also be useful to estimate the fatigue limit. In effect, phase can change due to the presence of either viscoplastic behavior of material[50,79] or high stress gradient, which leads to heat conduction and loss of adiabatic conditions.[13,15,108,109] Consequently, this loss of adiabaticity leads to shifts in the thermoelastic phase trend.

For a better explanation, Figure 13A shows the change in phase signal with four stress amplitudes, the first two are below the fatigue limit (around 170 MPa of ASTM A182) and the other are beyond the fatigue limit. As can be seen, a significant rise in the phase was observed when stress amplitudes exceeded the fatigue limit. This rise signifies the loss of adiabatic conditions and the damage occurrence.[47]

In TPA, the thermoelastic data were extracted during the second phase of the temperature trend in Loung's method where the average surface temperature remains constant.[47] For each loading step, the maximum phase change ($\Delta\varphi_{\max}$) was calculated by subtracting the maximum and minimum phase values during a certain thermographic sequence. Then, from the variation of $\Delta\varphi_{\max}$ with stress amplitudes, the fatigue limit can be found from a point where the curve experiences a sharp shift in its slope (see Figure 13B).[47]

A similar variation, ϕ_{EI} in Figure 14, was also reported by Cappello et al for C45.[110] Compared with the classical thermographic method ($\Delta T_{\max}$) in Loung's method, TPA showed superior performance for some materials or components that experience relatively low-temperature variations. It was reported that TPA outperforms methods based on only the stabilized temperature in materials with higher ductility.[47] In Figure 14, The green and blue cross marks show the minimum value (5th percentile) and the maximum value (95th percentile), which were changed with the loading amplitude.[110]

The reliability of the fatigue limit prediction using the phase shift data was examined by De Finis et al.[26] Furthermore, they showed that the sensitive behavior of the phase with the stress amplitudes[26] makes it a proper index to monitor the transition between the plastic and viscous phenomena and to describe the dissipative phenomena related to the plastic stress regime.

3.2.2 | Loss of linearity of FAH (first amplitude harmonic)

Krapez et al,[30,45] and later De Finis et al,[26,111] proposed similar temperature models to take advantage of using the first amplitude harmonic of the temperature. By comparing the first temperature amplitude with its linear trend evaluated at the beginning of the test, a significant difference was reported when the stress amplitude exceeded the fatigue limit. In other words, the TSA equation is no longer valid in the presence of damage when microplastic phenomena occur in the material. In these conditions, for a given stress level when the loss of linearity of the first harmonic is observed, the fatigue limit can be predicted. In Figure 15, full field maps of the first harmonic amplitude of temperature for C45 (with a fatigue limit of around 200 MPa) and its variation (E_I in[110]) are shown. Note that green and blue crosses in Figure 15 indicate minimum and maximum related values.[110]

As can be seen in Figure 15B, the nonlinearity occurred around 220 MPa, which is very close to the fatigue limit of the material.[30] It is worth noting that the intensity of the slope change of the curve depends on both the material and the stress ratio.[26,30]

3.3 | Energy-based approaches

Works on the relation between fatigue (or failure) and energy date back to the 1920s.[112] Nevertheless, it was not

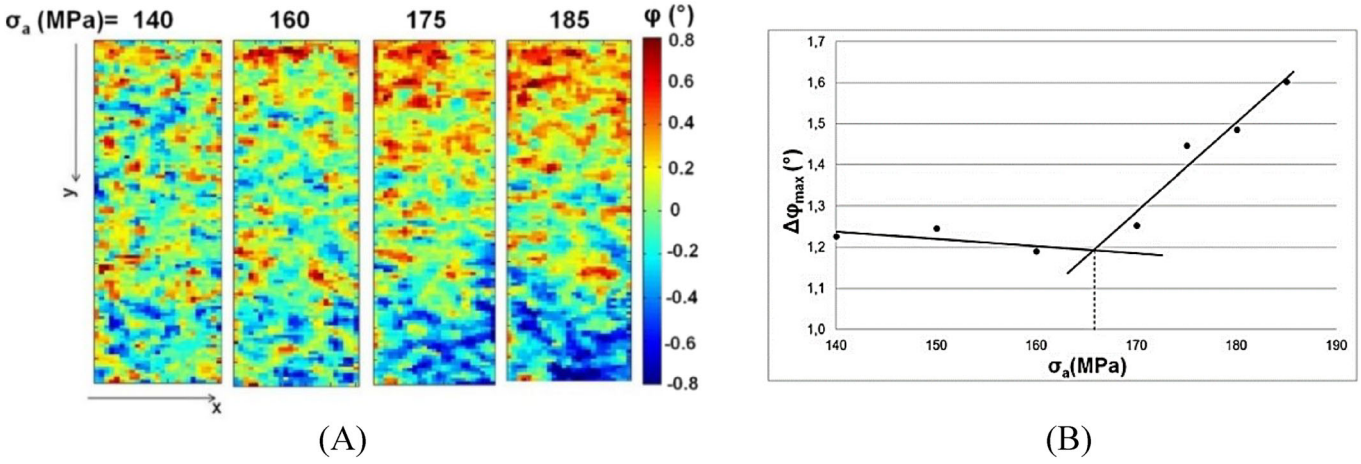

FIGURE 13 (A) Thermoelastic phase map for four different loading steps of ASTM A182 and (B) the maximum phase change curve.[47] [Colour figure can be viewed at wileyonlinelibrary.com]

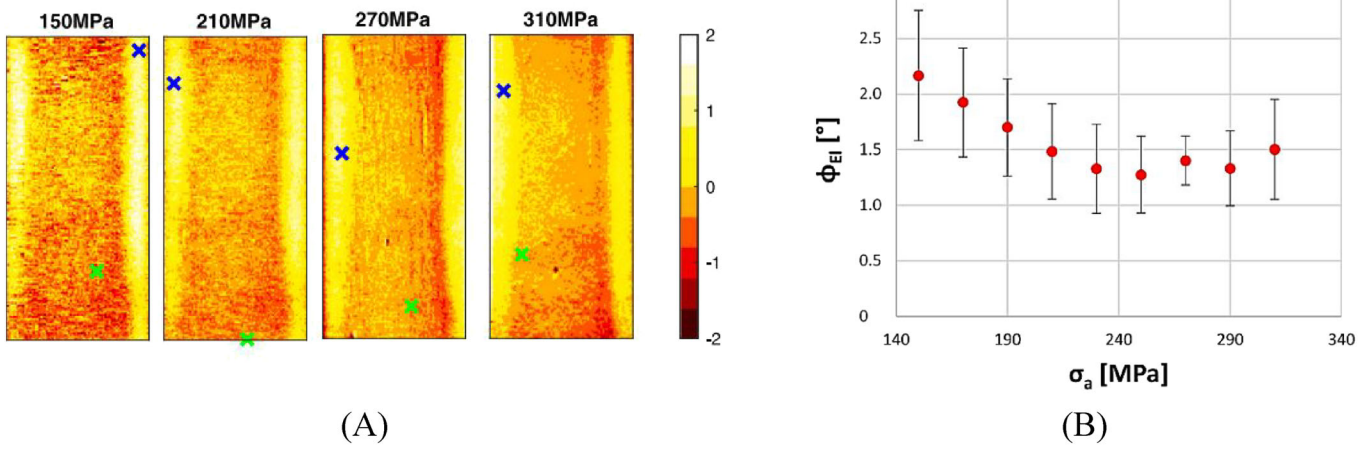

FIGURE 14 (A) Thermoelastic phase map for four different loading steps and (B) its variation for C45, $R = 0.1$.[110] [Colour figure can be viewed at wileyonlinelibrary.com]

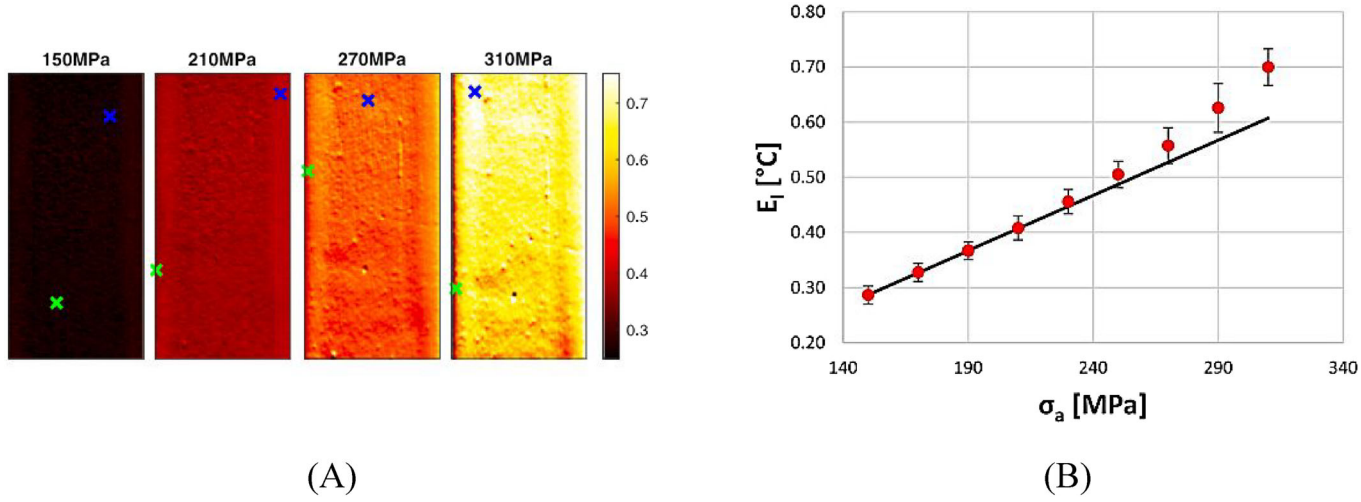

FIGURE 15 (A) First harmonic amplitude map for four different loading steps and (B) its variation for C45, $R = 0.1$.[110] [Colour figure can be viewed at wileyonlinelibrary.com]

until the early 1940s and 1950s that several researchers began to consider a correlation between the fatigue life of a material and the strain energy dissipation during the fatigue process.[17,69]

According to Feltner and Morrow,[17] Hanstock[113] likely first established a connection between strain energy density (SED) and fatigue life in 1947. Subsequently, in 1965, Morrow took a significant step by introducing a power function that relates plastic SED, plastic work, and fatigue life. This function can be regarded as the prototype of SED-based models in current use.[114] Subsequently, various forms of SED-based fatigue approaches were developed and enhanced.[114-117] Historical development of SED and a collection of equations directly correlating SED with fatigue life can be found in a work by Lia et al.[114]

A promising suggestion was that the strain energy needed for the failure of a material subjected to a static test is similar to the strain energy dissipated during a fatigue process.[30] As shown in Figure 16, the strain energy (or the normalized strain energy which is the strain energy density per cycle per the strain energy density in the steady-state strain region) rises with the number of cycles as plastic deformation or damage accumulated.[69]

3.3.1 | Second amplitude harmonics (SAH)

Enke and Sandor[44] showed how the evaluation of dissipative heat sources allows the assessment of the damage of material. Under the assumption of no significant mean strain (fully reversed cyclic loading), they introduced a general form of thermo-elastic-plastic response. They applied the Fourier sine series on the thermal signal obtained from an IR camera and mentioned that the amplitudes at the frequency and twice the frequency of the mechanical loading are proportional to the elastic and plastic strains (or deformation), respectively.

For a sinusoidal loading, a schematic description of the hysteresis loop with the variations of stress, strain, and temperatures is shown in Figure 17. From point "a" to "b," the elastic strain increases while the temperature simultaneously decreases, both following a sinusoidal pattern. In elastic unloading, from b to c, the temperature is due to only elastic deformation (T_{elastic}). This behavior is repeated for c–d and d–e but with opposite signs for elastic temperature contribution. As reported clearly by Enke and Sandor,[44] for each cycle of elastic temperature response, two cycles of plastic temperature response occur. Therefore, twice the frequency of loading, 2f, plays a fundamental role in assessing T_{plastic}. Note that at the beginning of the test, this temperature contribution is negligible, while it increases with plastic deformation and damage. As an example, the full field maps of the second harmonic amplitude of temperature (D_I in[110]) for C45 with the fatigue limit of around 200 MPa are shown in Figure 18.

In addition to the previous studies, Krapez et al[30,45] showed that the energy variations produced by irreversible processes produce a second harmonic temperature component as a fatigue indicator. They studied the thermal signal in the frequency domain to separate both the dissipative and thermoelastic sources.[30,45] The idea was first suggested by Bremont and Potet.[31]

To improve the accuracy of the measurement of the dissipated energy, Shiozawa et al[32,118] proposed a

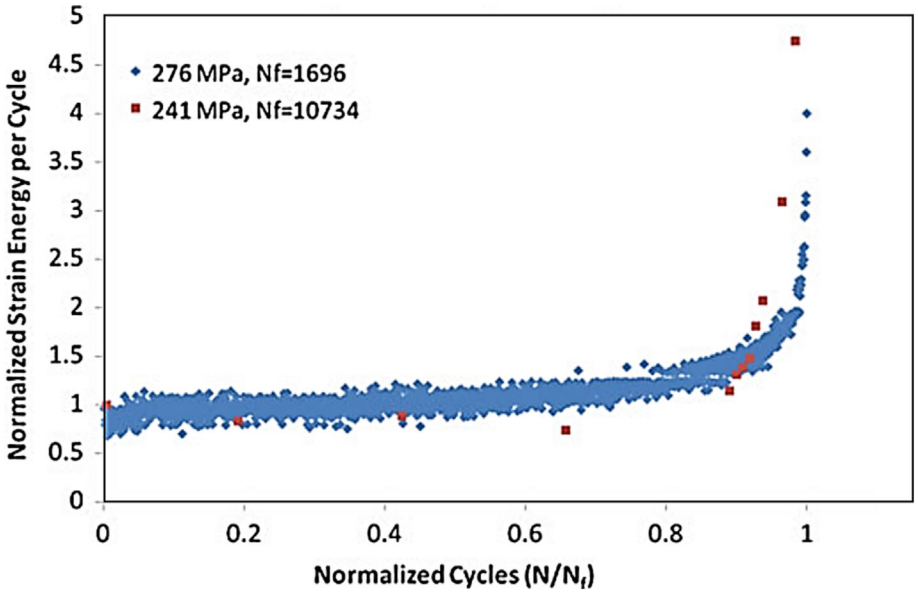

FIGURE 16 Normalized strain energy variation during the fatigue test for Al 6061-T6[69] [Colour figure can be viewed at wileyonlinelibrary.com]

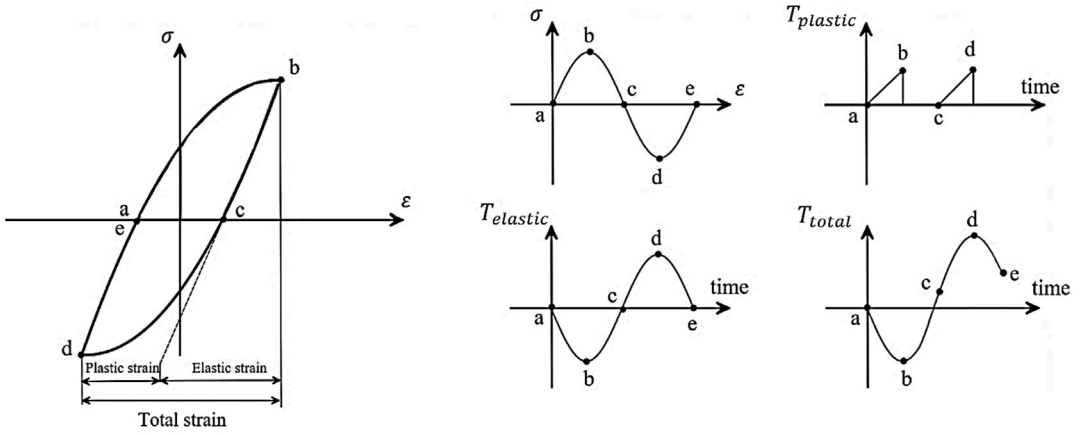

FIGURE 17 A schematic representation of hysteresis loop and temperature variations during a single cycle under sinusoidal stress (redrawn based on Enke and Sandor[44]).

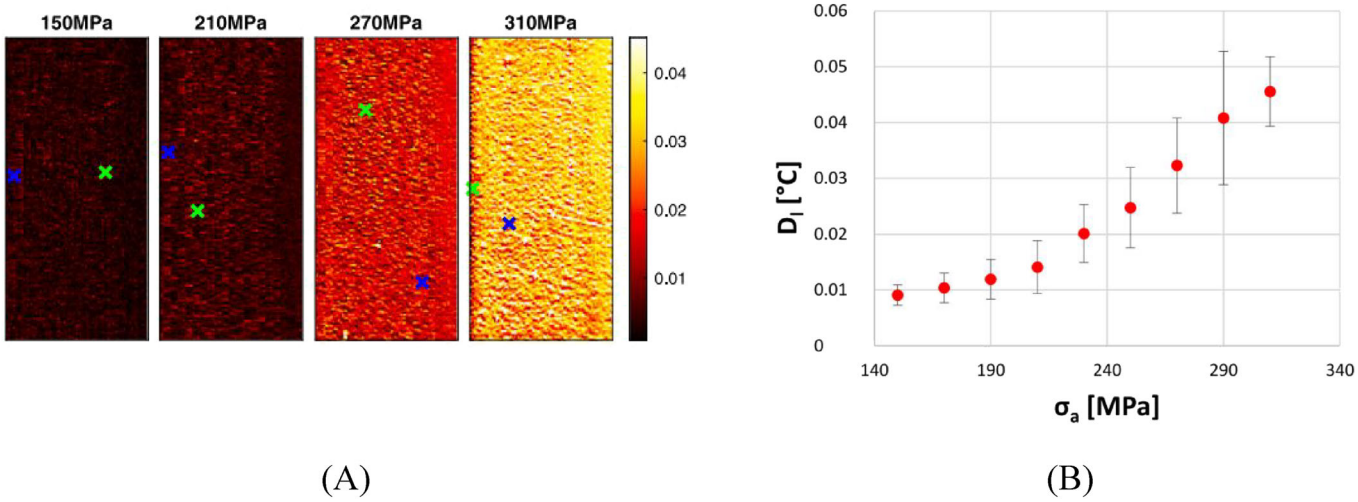

FIGURE 18 (A) Second harmonic amplitude map for four different loading steps and (B) its variation for C45, $R = 0.1$.[110] [Colour figure can be viewed at wileyonlinelibrary.com]

technique that benefits from the phase 2f lock-in IR method. It works with a double frequency component of temperature change, which includes the influence of both energy dissipation and thermoelastic source (see Figure 4B). This technique effectively eliminates the superficial portion of dissipated energy (or generally the noise components) related to thermoelastic temperature, ΔT_E, caused by the harmonic vibration of the loading machine. The aim was to find the real temperature rise due to the energy dissipated, ΔT_d, and the energy dissipated rate, q. They are formulated as follows:

$$\Delta T_E = -kT\Delta\sigma, \tag{7}$$

$$q = \rho C_p \Delta T_d, \tag{8}$$

where k is the thermoelastic coefficient, T is the absolute temperature, and $\Delta\sigma$ is the sum of principal stresses.

Further investigation in the SAH of temperature, ΔT_{2w}, was carried out by De Finis et al.[72] Particularly, the capability of ΔT_{2w} signal as an indicator to predict the heat dissipated energy was studied. Additionally, they found a relationship between SAH of heat dissipated rate $\Delta\dot{E}_{d_{2w}}$ and mechanical energy rate $\Delta\dot{W}_{2w}$ for C45 steel under two stress ratios, $R = 0.1$ and -1, as follows:

$$\Delta\dot{W}_{2w} = A_1\Delta\dot{E}_{d_{2w}} + A_2, \tag{9}$$

where A_1 and A_2 depend on the material. While the first one was reported to be dimensionless, the second dimension has the same as either $\Delta\dot{W}_{2w}$ or $\Delta\dot{E}_{d_{2w}}$.

The endurance limit can be estimated from the latter one, $\Delta E_{d_{2w}}$,[119] and subsequently the area under the hysteresis loop. However, the accuracy of this approach depends on the following assumptions, (i) the full conversion of the mechanical energy into heat, (ii) the consideration of only a fraction of ΔE_d, and (iii) the determination of $\Delta E_{d_{2w}}$ from ΔT_{2w} on the surface, which is smaller than the value related to the actual heat source. Furthermore, a framework was analytically developed and experimentally validated by Meneghetti and Ricotta[73,120] to provide a correlation between intrinsic dissipation and the second amplitude harmonic.

3.3.2 | Specific heat loss

Meneghetti[43] introduced another promising parameter for fatigue characterization based on the energy per cycle in a unit volume, rather than the surface temperature. Using the energy balance equation, a relationship between thermal power dissipated per unit volume (including conduction, convection, and radiation) and the cooling rate ($\partial T/\partial t$). It was found from the temperature evolution curve after a sudden interruption of the fatigue test, see Figure 19.

After finding the cooling rate from experimental measurements, the heat dissipated was calculated[43,74] as follows:

$$\dot{Q} = -\frac{\rho C}{f}\frac{\partial T}{\partial t}\bigg|_{t=t^*} \tag{10}$$

where ρ and C represent respectively the mass density and the specific heat and f is the frequency. This heat loss only depends on the applied cyclic loading characteristics: mean, amplitude, and stress state. Applicability of this method can be found in the literature for different steels and fracture mechanics approach.[121-123] As an example, for AISI 304 L stainless steel, the fatigue limit predicted based on the thermal energy dissipated or the cooling gradient is shown in Figure 20.

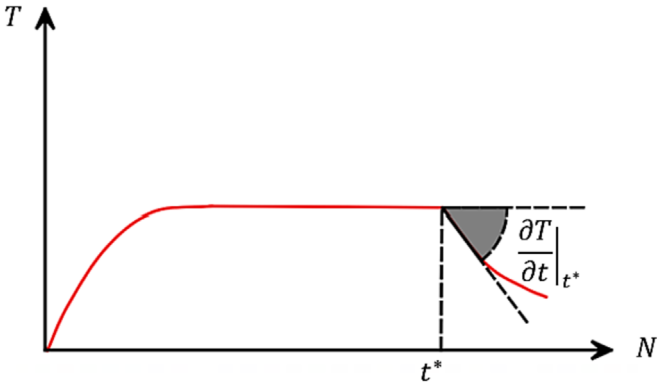

FIGURE 19 Slope of the cooling rate. [Colour figure can be viewed at wileyonlinelibrary.com]

For a given material, loading, and mechanical boundary conditions, the surface temperature depends on the geometry of the sample, the loading frequency, and the heat exchange from the material to the surroundings. However, the dissipated energy is only dependent on the applied stress amplitude and load ratio. Therefore, surface temperature cannot be adopted for geometries and testing conditions different from the reference ones.[43]

Rigon et al[125] showed that the cooling gradient just after t^* is at least one order of magnitude higher than the heating gradient at the same time. Therefore, the dissipated fraction is far greater than the self-heating portion of the total heat production. Furthermore, in a more recent study, Rigon et al[34] successfully applied the method to fatigue tests under in-phase and out-of-phase axial/torsional multiaxial loadings. It is worth mentioning that the thermographic technique is mainly carried out in uniaxial fatigue tests where the occurrence of temperature stabilization is feasible. However, this assumption cannot be always made in the case of multiaxial loadings which is not the focus of this paper. For further information on the applicability of thermography in fatigue life prediction under multiaxial and non-proportional fatigue loadings, readers can refer to the work by Skibicki et al.[126]

3.3.3 | Entropy-based methods

Based on the thermodynamic theory of irreversible process, as Naderi et al[127] proposed, the entropy generation during the fatigue test can be regarded as a degradation index. According to this work, entropy accumulates until it reaches a specific value known as the fatigue fracture entropy (FFE), which is defined as follows:

$$\gamma_f = \int_0^{t_f}\left(\frac{W_p}{T} - \frac{q.grad\,(T)}{T^2}\right), \tag{11}$$

where γ_f is the FFE, t_f is the time up to the fatigue failure, and q is the heat flux across the boundary. An IR camera was used to record the temperature evolution, T, during the entire test and the plastic energy, W_p, determined by Morrow's cyclic plastic energy dissipation formula.[128] As an example, the evolution of the rate of entropy flow of aluminum 6061 up to failure is shown in Figure 21A.

In low-cycle fatigue where the entropy generation is dominantly due to the plastic deformation, the second

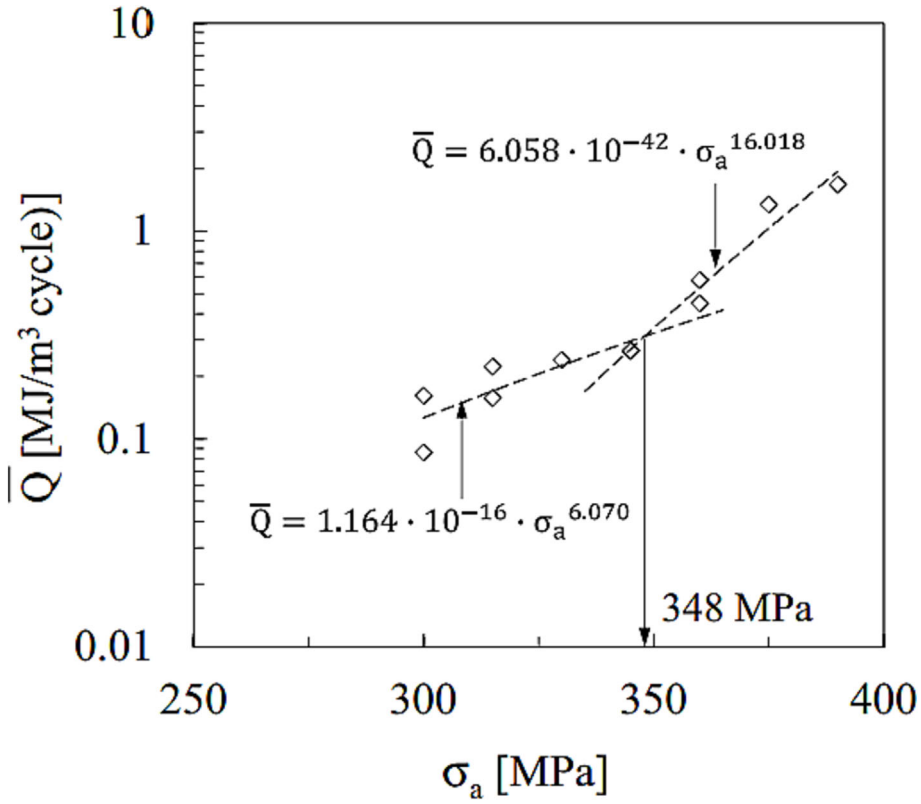

FIGURE 20 Fatigue limit prediction with thermal energy dissipated or the cooling gradient for AISI 304 L stainless steel.[124]

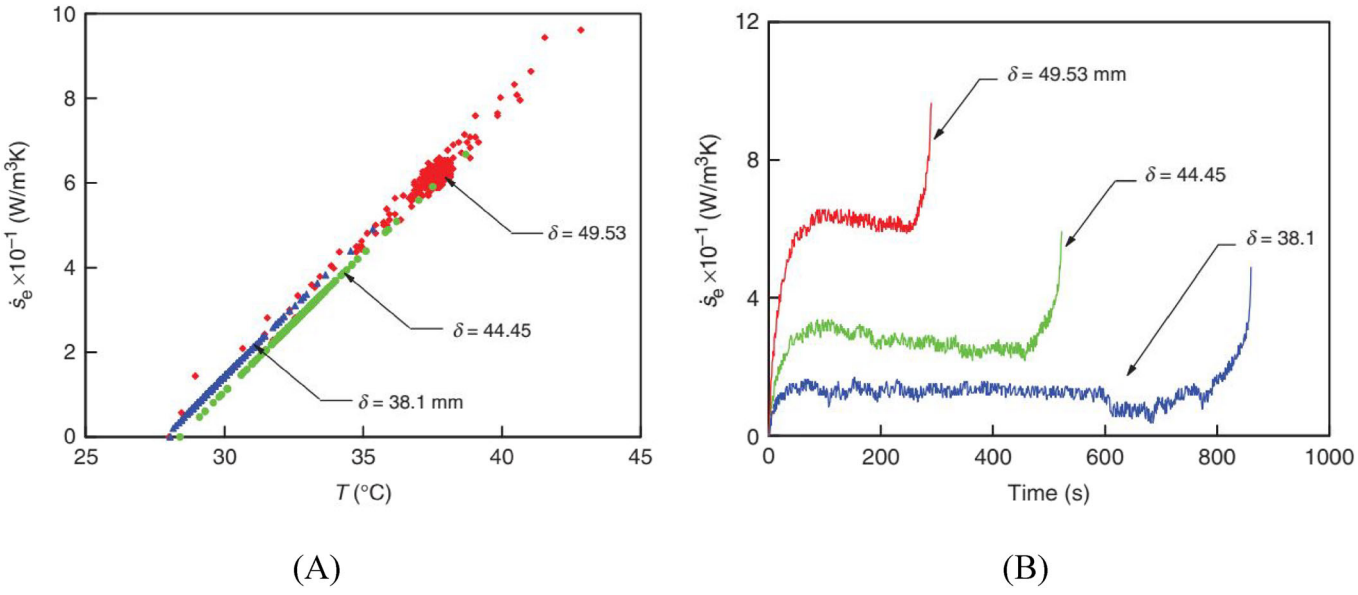

FIGURE 21 Evolution of rate of entropy flow of aluminum until failure occurs: (A) Variation with temperature and (B) variation with time.[82] [Colour figure can be viewed at wileyonlinelibrary.com]

term in the integral was shown to be negligible.[98] It was verified that γ_f is a material constant, independent of the geometry as well as load and frequency.[98]

As can be seen from the temperature trend in Figure 21B, after the steady state phase, entropy increases sharply at around 90% of the fatigue. This behavior aligns with the temperature slope shown in Figure 10. From this observation, Naderi and Konsari[129] stated that the operation, or loading, should be continued until $\gamma \leq 0.9\gamma_f$, avoiding fracture.

In other studies, it was shown that the cyclic energy dissipation in the form of thermodynamic entropy can be

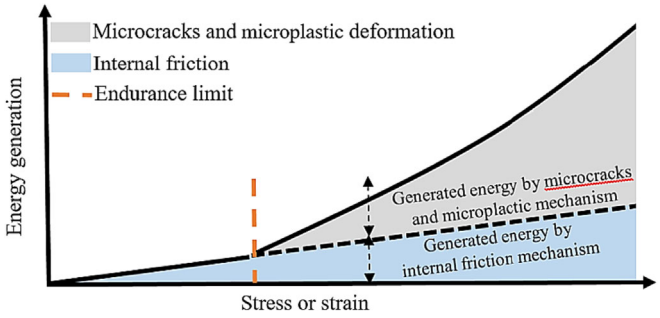

FIGURE 22 The schematic diagram of energy generation as a function of stress or strain showing the contribution of microplastic and internal friction.[131] [Colour figure can be viewed at wileyonlinelibrary.com]

effectively used to calculate the evolution of the fatigue damage[82] and the remaining life.[49] Through an experimentally verified analytical approach, Jang and Khonsari[130] showed that the energy dissipation caused by the recoverable internal friction should be removed from the irreversible microplastic deformation (see Figure 22) to precisely find the FFE value.[130,132-134]

3.4 | Thermoelastic point inversion assessment

A different approach has been adopted by Risitano and Risitano[52] to estimate the fatigue limit, assessing the end of the thermoelastic effect during a static test, a methodology that they referred to as the "Static Thermographic Method."

As Risitano and Risitano mentioned, a static tensile test can be considered a part of the initial cycle of a fatigue test under fully reversed loading. Thus, it is possible to find the stress amplitude related to the fatigue limit by monitoring the surface temperature changes during a static test.[52] It is worth pointing out that this method was inspired by the work of Bottani and Caglioti[135] to some extent while primarily relying on the research by Plekhov and Naimark[38] and Risitano et al.[136]

Generally, the thermal behavior of metals or crystalline solids under tensile test can be distinguished by two distinct zones: the elastic zone with linear stress–strain relationship and the plastic zone where not all crystals deform within an elastic field.

They proposed that during tensile tests, fatigue failures happen at points in the material's stress–strain curve where the local stress is able to produce plastic deformation.[52] These localized stresses intensify compared to the average applied stress (load/area), leading to fatigue failure. Therefore, the specimen fails when the load surpasses this average value.[52] This value can be identified when the linear trend of the maximum surface temperature in Figure 23 (thermoelastic behavior) is lost.[52]

This non-linearity happens due to the fact that the local intensified stress causes irreversible microplastic deformations (Zone II in Figure 23) and consequently heat dissipation.[52] They mentioned that except for some crystals which are deformed plastically, most of them are stressed in an elastic field. Conversely, plastic deformation intensifies within Zone III, ultimately encompassing every crystal in Zone IV.[52]

In another work, Risitano et al[137] showed that the method is dependent on the stress rate applied during the tensile test. However, this dependency does not impact the results achieved in terms of the fatigue limit. The method can be conducted even with a limited number of specimens and within a short timeframe.[19,138-140] Nonetheless, for a robust estimation of the fatigue limit, it is advisable to test at least five samples.

4 | PROCEDURE, TYPICAL SETUP, AND EQUIPMENT USED FOR RAPID FATIGUE TESTS

4.1 | Experimental setup

The typical experimental arrangement includes an IR camera and a set of computer-controlled components, as shown in Figure 24. Tests are conducted using a mechanical excitation source, which is supplied by a servo-hydraulic testing machine equipped with an appropriate load cell capacity. The testing environment is maintained at an almost constant temperature. Samples should be sized based on the available standards[141] and typically have a dog bone or hourglass geometry.

As can be seen in Figure 24, a computer collects both the load cell signal, which serves as the reference signal for the noise rejection process, and the thermographic signal. Following this, the software calculates temperature from the IR signal and presents it as colorful temperature maps.

The testing procedure includes a sequence of loading blocks, each with the same duration of loading cycles, and fixed values for loading frequency and stress ratio.[25] This process continues until the material eventually fails. As proposed in Figure 25, the sequence of loading blocks is defined by incrementally increasing the applied stress level, in a procedure known as stepwise loading.

As mentioned before, each block includes a specific number of cycles, and after completing each block, the stress is increased until the material fails. For the first block, it is suggested that the maximum stress should be

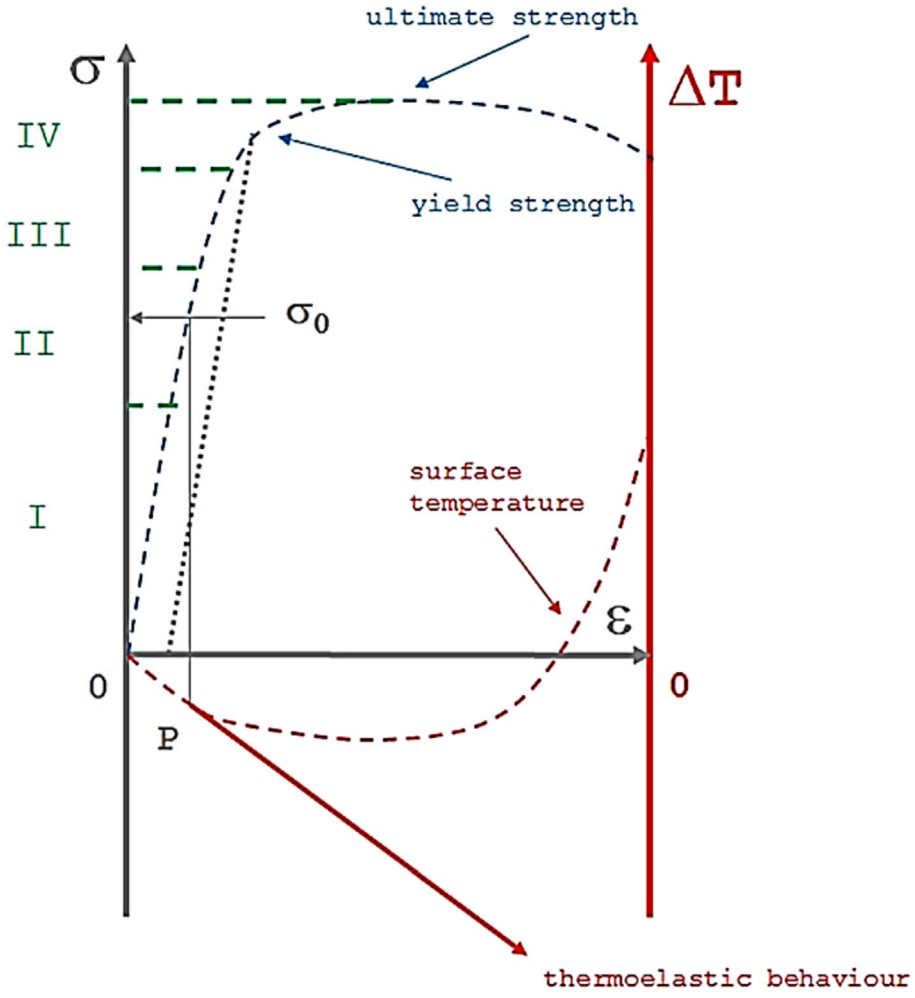

FIGURE 23 Qualitative stress–strain and temperature–strain curves.[52] [Colour figure can be viewed at wileyonlinelibrary.com]

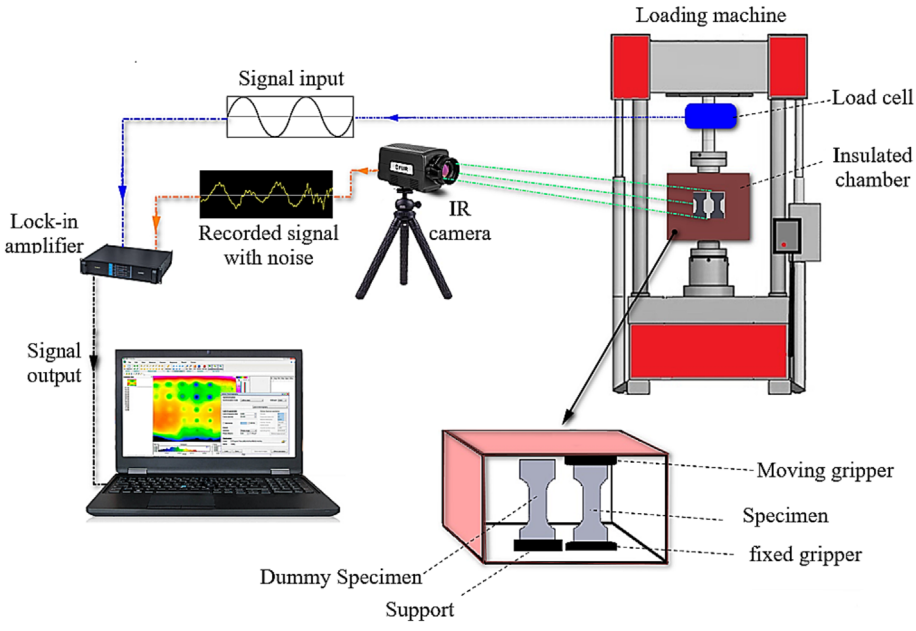

FIGURE 24 Experimental setup for the rapid fatigue test. [Colour figure can be viewed at wileyonlinelibrary.com]

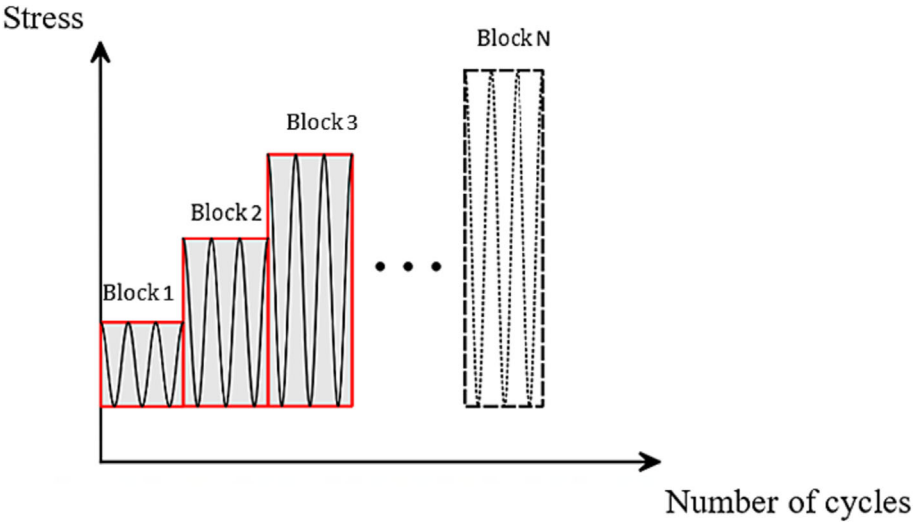

FIGURE 25 A schematic of stepwise loading. [Colour figure can be viewed at wileyonlinelibrary.com]

20%–30% of the ultimate tensile strength of the material to ensure collecting enough data below the fatigue limit.[142] The stress increment between each block can be varied but should be set such that the total test duration remains practical while still collecting a satisfactory number of data points around the fatigue limit.[119]

During each block, thermographic acquisitions are performed for a predefined time period and sampling frequency. Certainly, the quality of the thermal acquisition depends on the camera specifications (i.e., cooled or uncooled) and settings (e.g., the frame rate, the integration time, and the temperature range).

Generally, the Thermographic method[25] requires a continuous temperature acquisition, which can be accomplished using a typical uncooled microbolometer camera. However, a cooled camera is essential if the objective of the test is extracting harmonic components of the temperature. For this purpose, the thermal signal should be properly reconstructed, which needs higher acquisition frame rates. One way to implement all the presented approaches for fatigue assessment is utilizing both cooled and uncooled IR detectors simultaneously.[21,22,25] Interested readers can find a comprehensive comparison between cooled and uncooled cameras in a study by Deane et al.[143]

Key factors that significantly impact measurement accuracy are classified into three groups, as described in the work by Bagavathiappan et al.[144]

The first group consists of operational factors, which relate to the available information and experiences about the test conditions and samples. The involvement of skilled thermographers can help to minimize these factors, resulting in better thermal images from the region of interest.

Technical factors make up the second group, including variables such as the emissivity of the object under investigation and the distance between the camera and the object. The emissivity is considered as an effective parameter in the measurement. To address this, samples are usually covered by a layer of black paint of appropriate thickness. This coating increases their emissivity and prevents reflections caused by heat sources in proximity to the samples during the test.

The final group contains environmental factors, including ambient air temperature, humidity, and convention. To minimize these effects, it is advisable to enclose samples in an insulating chamber if it is possible.[25] Furthermore, placing a dummy-unloaded specimen made from the same material as the tested inside the insulated chamber provides a temperature reference.[47]

Table 1 outlines the necessary experimental conditions to obtain various thermal indices. It is worth noting that the experimental setup required for obtaining the thermal indices is similar to the one explained earlier, with specific requirements for each index presented below.

From Table 1, the first consideration refers to the use of an appropriate IR camera to acquire suitable data for a specific thermal index. In contrast to the mean temperature-related indices (i.e., indices 1, 2, and 6, corresponding to the mean temperature increase, the initial slope of the temperature, and specific heat loss), which require a typical low-cost uncooled camera, the acquisition of harmonic components of the temperature (indices 3, 4, and 5, corresponding to the thermoelastic phase, first amplitude harmonic, and second amplitude harmonic) needs a high-performance cooled camera.[42,43,47,72,144]

The second row of Table 1 regards the sample rate used for capturing the thermal sequence. Unlike indices 1, 2, and 6, which do not necessitate a high frame rate, thermal indices 3–5 require a higher frame rate. This

TABLE 1 Experimental requirements for the acquisition of different thermal indices.

Requirements			Thermal indices 1: Mean temperature increase	2: Initial slope of the temperature	3: Thermoelastic phase	4: First amplitude harmonic	5: Second amplitude harmonic	6: Specific heat loss
1	IR Camera	Uncooled camera	X	X				X
		Cooled camera			X	X	X	
2	High frame rate				X	X	X	
3	High loading frequency					X		
4	Dummy specimen		X	X				
5	Insulating chamber		X	X	X	X	X	
6	Thermal acquisition type	Continuous	X					
		Discrete		X	X	X	X	X

increased frame rate is crucial because it ensures the accurate reconstruction of the temperature signal, which is a fundamental requirement for obtaining the aforementioned indices.[26,30,111]

Furthermore, from the third row of Table 1, when acquiring the first harmonic amplitude, it is important to conduct the test at a high loading frequency. This ensures the adiabatic condition during the initial loading stages and allows for the observation of linearity loss caused by damage.[15,145,146]

From the fourth row of Table 1, a dummy pristine sample should be included when the first two indices are chosen to eliminate the environmental temperature effect from the mean surface temperature of the sample.[47] For all indices except the specific heat loss, the use of an insulating chamber is recommended to reduce the influence of environmental factors.[119,147]

The last consideration is the way each index should be captured. As shown in Table 1, except for the mean temperature index, which needs to be acquired for the whole of the temperature trend, the other indices can be captured discretely by considering suitable time windows during the test.[22,26,27,81,110]

4.2 | Thermal signal processing

La Rosa and Risitano[22] and Luong[21] were the first to perform signal processing on the mean temperature acquired from the surface of the specimen by the thermography technique. This process involved subtracting the environmental temperature from the mean temperature.

A more complicated signal processing was conducted by Krapez et al,[30] which involves the assessment of harmonic components of a thermal signal in terms of amplitudes and phases. Indeed, Krapez was the first to deeply investigate the thermal signal by examining the harmonic components of the temperature signal. A particular signal demodulation procedure was used to extract the first two Fourier components and the mean temperature rise of some stainless steel and aluminum alloys. They found experimentally that for stress amplitude roughly close to the fatigue limit, three phenomena occur: (i) a significant increase in the mean temperature; (ii) a sharp change in the slope of the thermoelastic curve (representing the temperature component at the frequency of loading and stress amplitude); and (iii) the appearance of the temperature component at twice the frequency of the loading (2f). This procedure is called Lock-in[74] because it needs a reference signal (load or strain) for processing the temperature field via the fast Fourier transform (FFT). With lock-in thermography, all aforementioned phenomena can be captured [50]. Krapez et al[30] modeled the temperature as follows:

$$T(t) = T_0 + \Delta T f t + T_1 \sin(\omega t + \varphi_1) + T_2 \sin(\omega t + \varphi_2), \tag{12}$$

where f is the loading frequency, T_0 is the temperature level at the beginning, ΔT is the mean rise of the

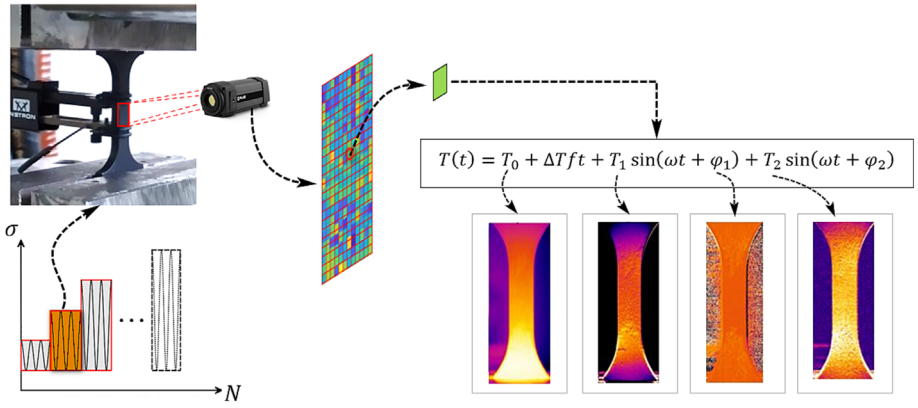

FIGURE 26 From the thermographic signal to temperature components acquisition. [Colour figure can be viewed at wileyonlinelibrary.com]

temperature per cycle. T_1, φ_1, T_2, and φ_2 are the amplitudes and phases associated with the first and second Fourier components. A schematic presentation of the above thermal signal processing is shown in Figure 26.

Note that the above model can also be implemented in the least square method for thermal signal reconstruction.[30] To improve the signal-to-noise ratio, the temperature maps in the central part of the sample or a region with a particular thermal behavior were averaged. It should be noted that in contrast to Risitano's method, which is based on the mean temperature, analyzing the first and higher harmonic orders of the temperature signal is based on the amplitude and phase. Therefore, thermal cameras with higher frame rates are necessary.[40,74]

As explained by De Finis et al,[26,111] T_1 shows the stress field on the surface of the sample, reflecting the signal variation or thermoelastic effect, while T_2 is proportional to the intrinsic dissipation energy. ϕ can be related to various factors including the loss of the adiabatic condition, plastic deformation, damage, and surface treatment. The change of these parameters with respect to the stress amplitude was used to probe into the thermoelastic and plastic behavior of the material, the fatigue behavior of materials[148] especially with high diffusive behavior like aluminum,[142] and estimating the fatigue limit.[26,111]

5 | METHODS FOR RAPID ESTIMATING OF THE FATIGUE LIMIT

In the present section, the focus is on the well-established methods used for estimating the fatigue limit in a rapid way. It begins with the pioneering approach and then provides an overview of recent developments in this area. In fact, there are only a few methods available for rapid fatigue limit estimation: the thermographic method by Luong–Risitano or referred also to as Luong's method",[22,81] the "iterative method" by Curà et al,[39] the "threshold method" by De Finis et al,[25] and the "thermoelastic point inversion" by Risitano and Risitano.[52]

5.1 | Luong–Risitano's method

As mentioned before, in this method, the stabilization temperature serves as a fatigue parameter. By plotting the curve of the stabilized temperature for each stress magnitude (see Figure 8), La Rosa and Risitano[22] expressed that the fatigue limit can be achieved by indicating a point on the curve where a sharp change in the slope occurs. An interesting aspect of this method is that it lasts only a few cycles to reach the stabilization temperature, the entire process usually encompasses just 10% of the specimen's entire lifespan. Therefore, it is possible to use the same specimen for different levels of loading; because the cumulative damage is considered negligible up to temperature stabilization.[27,29]

Furthermore, as La Rosa and Risitano mentioned,[22] only three specimens are sufficient to estimate the fatigue limit because the data show minimal scattering. As shown in Figure 27, through plotting the temperature related to high dissipation (observing from the surface of the sample) with the stress level, Loung noticed a breakpoint (i.e., a point with sharp slope change), which can be used for fatigue life prediction.[21,81]

5.2 | Iterative method

Curà et al,[39] proposed another rapid method based on the stabilization temperature for the determination of the fatigue limit of materials (mild steel Fe 510 in their study) and components based on the Luong approach.[21,81] As shown in Figure 28, the method initially involves selecting a trial stress magnitude to separate the thermal data into two groups, below and above the stress value. Next, two straight lines are fitted to interpolate each group of

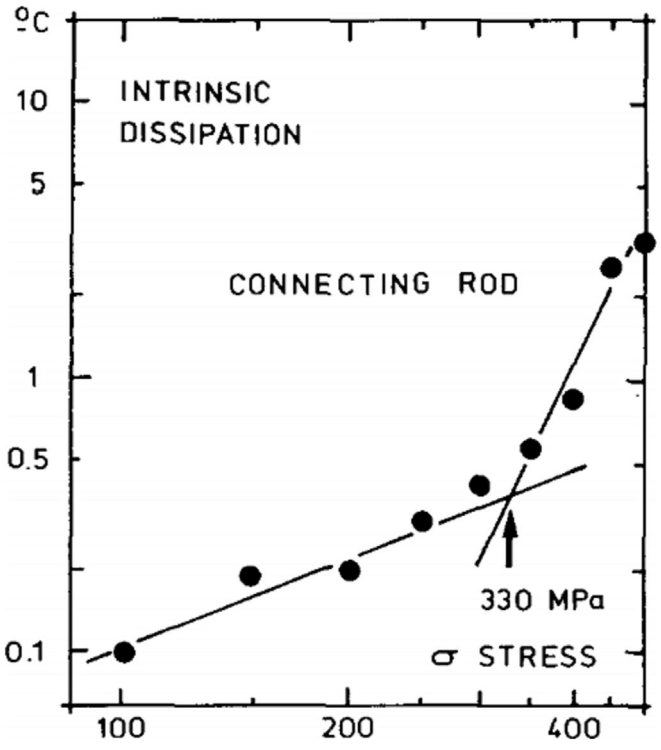

FIGURE 27 Graphical determination of the fatigue limit of steel by Luong.[81]

data in the space of temperature difference and stress amplitude. The intersection of these two lines shows a trial fatigue limit.

Here is where the iteration process comes into play. If the difference between the trial stress and estimated fatigue limit is positive, the next trial stress must be selected lower than the first one, and vice versa. The process of selecting a trial stress and finding the trial fatigue limit continues until the difference between them falls below a predefined threshold. When this condition is met, the trial stress is considered a reliable estimation of the fatigue limit.

On the contrary, in Luong's method, there is not any trial-and-error procedure. Once the first intersection point is found, its corresponding stress value indicates the fatigue limit. Therefore, the accuracy of the iterative method is highly dependent on the chosen trial stress.

5.3 | Threshold method

Another method for rapid estimation of fatigue limit was introduced by De Finis et al.[25] They managed to approximate the temperature changes due to the damage by removing the effects of the environment and loading machine. For this purpose, a linear function of stress amplitude with two constants was introduced. These constants were initially identified by fitting a line to the experimental data during the initial loading stages and were then used as known values for the next steps.

As shown in Figure 29B, they showed that when the difference between the maximum temperature change (or steady state temperature) acquired from the surface by an IR camera and the linear function, exceeds a threshold value, fatigue failure is likely to happen; this difference called "residual of the temperature," $\Delta T_{\max\_r}$. The threshold value was defined as six times the standard deviation of residuals for the first five experimental data ($\Delta T_{h\_6\sigma}$).

Moreover, as shown in Figure 29B, in contrast to Luong's method[81] in Figure 29A, it is not necessary to continue the test up to the failure in order to evaluate the fatigue limit.[25] As they mentioned, the threshold method can be used to determine the transition that occurs in the behavior of the material.[25]

5.4 | Thermoelastic point inversion in tensile test

According to the work by Risitano and Risitano,[52] if the temperature curve is added to the typical stress–strain curve (see Figure 30), it becomes feasible to find a limit temperature that marks the beginning of the nonlinearity of the temperature curve. The corresponding stress value associated with this limit temperature can be regarded as a good estimation of the fatigue limit.

From Figure 30, the temperature evolution is characterized by three zones. Initially, there is an approximately linear decrease, mainly due to the thermoelastic effect. Subsequently, non-linearity emerges as mechanical energy is transformed into heat, signifying the initiation of microplastic deformation, and this phase reaches a minimum temperature value. Finally, the temperature starts to rise, ultimately leading to material failure.

6 | DISCUSSION AND OPEN POINTS

In this section, the thermal fatigue indicators and thermographic methods as well as their respective pros and cons and related unresolved issues are discussed. Table 2 summarizes all the parameters utilized in the literature for estimating fatigue limit. References to pioneering and relevant works for each parameter, along with the associated procedures, are indicated. It is worth mentioning that both temperature and energy-based parameters are suitable to be implemented in the procedures presented in the previous section to estimate the fatigue limit.

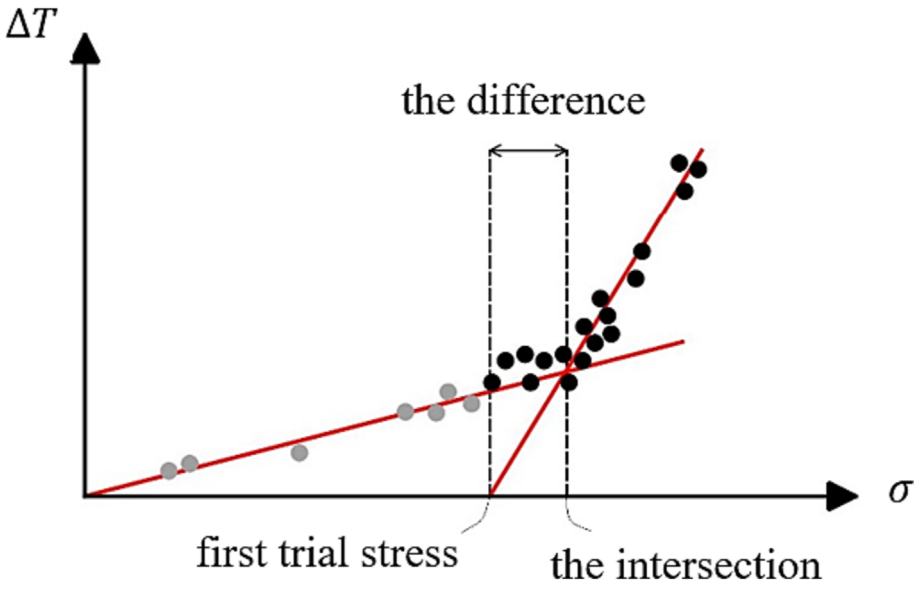

FIGURE 28 Schematic representation of Curà et al method. [Colour figure can be viewed at wileyonlinelibrary.com]

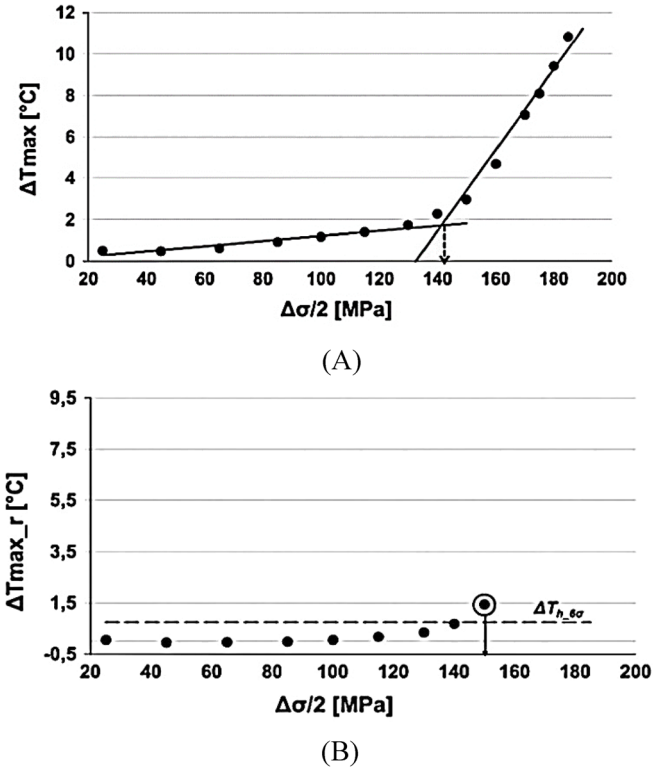

FIGURE 29 Comparison between (A) Luong's method and (B) threshold method for ASTM a 182 grade F6NM.[25]

6.1 | Capabilities of each thermal index for fatigue assessment

In the present section, the capability of all studied thermal indices is investigated according to different factors that can affect the measurement and/or the analysis. To enhance simplicity and readability, Table 2 is proposed to summarize this investigation; each index is numbered as follows:

1. mean temperature increase
2. initial slope of the temperature
3. thermoelastic phase
4. first amplitude harmonic of temperature
5. second amplitude harmonic of temperature
6. specific heat loss

Referring to the sensitivity to the heat diffusion effect (the first row in Table 3), the methods relying on the direct measurement of the temperature, such as the mean temperature, encounter difficulties when dealing with materials exhibiting high diffusivity. Indeed, the temperature variations, especially the mean temperature variations, can be extremely subtle and challenging to measure even with high-performance equipment such as IR-cooled cameras.[22,25,39,81] Indices 3, 4, and 5, which rely on either the harmonic amplitudes[26,30,32,45,72] or the phase information,[47] are likely the most accurate for fatigue limit estimation. This is because they involve a postprocessing analysis of the thermal data.

As explained below, various studies demonstrate their superior performance in comparison to the mean temperature. Kawai et al[149] conducted a study comparing the performance of the mean temperature and the second amplitude harmonic. They clearly stated that, unlike the latter, the mean temperature should not be used in high-stress concentrated parts. The reason is the formation of a significant temperature gradient between the region

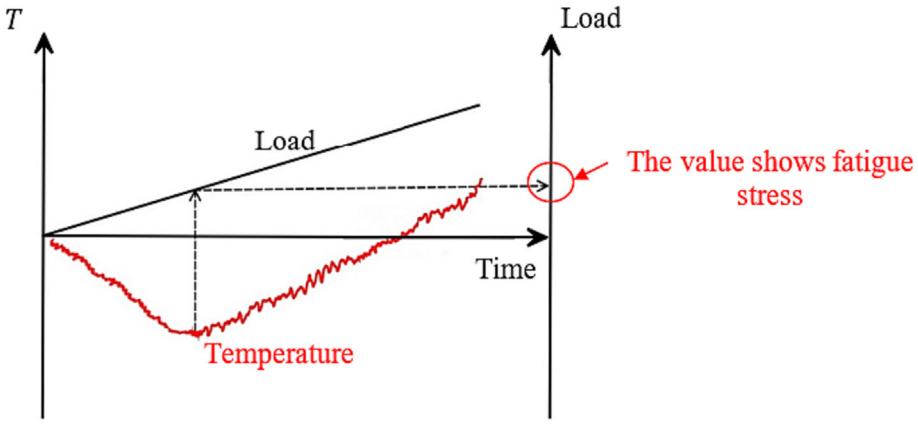

FIGURE 30 Fatigue limit prediction from tensile test. [Colour figure can be viewed at wileyonlinelibrary.com]

with stress concentration and its surroundings. By increasing the load level, this gradient becomes more pronounced, leading to the distortion in the correlation between load amplitude and the mean temperature, which, in turn, affects the fatigue limit evaluation.[149] In another work, De Finis et al,[148] showed the effectiveness of the second harmonic amplitude and thermoelastic phase in martensitic stainless steels, where the martensitic microstructure leads to stress concentrations during cyclic loading. In addition, in a more recent work by Lepitre et al,[150] the reliable performance of the first amplitude harmonic in fatigue crack detection of steel was demonstrated.

From the second row of Table 3, the microstructure of the material presents another limitation for fatigue limit prediction with certain indices. Among them, index 3 stands out as the only one with almost insensitive behavior to this problem.[47] As explained by Palumbo and Galietti,[47] this sensitivity can be due to the fact that the heat generation and the maximum temperature that can be achieved during the test are considerably lower when dealing with brittle materials. Consequently, accurate data processing becomes essential to extract the signal from the noise, in this case.

Concerning the effect of the environmental conditions, as placed in the third row of Table 3, all indices based on the mean temperature, except for the specific heat loss index, show sensitive behavior. However, the harmonic components have been reported to exhibit less sensitivity compared to the others. Since they are analyzed in the frequency domain which effectively filters out the impact of environmental factors.[26,32]

Of course, there are other factors that can affect the above indices, but the influence is almost the same for all considered indices. These factors can be the inaccuracy associated with the assumption that the surface temperature is representative of what happens throughout the thickness, the material geometry, loading frequency, loading ratio, and the heat conduction produced by the hot oil in the loading machine gripper.[124,151]

1. mean temperature increase
2. initial slope of the temperature
3. thermoelastic phase
4. first amplitude harmonic of temperature
5. second amplitude harmonic of temperature
6. specific heat loss

Considering the information summarized in Table 3, it can be concluded that the presented parameters can be also used in synergy to obtain complementary information for fatigue characterization, enabling the selection of the most suitable one for a specific test condition.

6.2 | Accuracy and uncertainty in predicted fatigue limit by thermographic methods

First, in this section, the accuracy of different methods in the fatigue limit estimation is examined. Four rapid methods for fatigue limit estimation are compared, which include (I) Loung-Risitano's method,[22] (II) the iterative method[39] (III) the threshold method,[25] and (IV) the thermoelastic point inversion method in tensile test,[52] are compared with the traditional method of fatigue limit prediction, the staircase method, to investigate their effectiveness. Next, the uncertainty in the predicted fatigue limit is discussed based on some features.

As can be seen in Table 4, methods (I)–(III) can estimate the fatigue limit very close to those determined by the staircase method.[22,25,39] However, it is worth highlighting that, as suggested by Risitano et al,[137] the estimated fatigue limit using method (IV) is considerably below the traditional staircase procedure, essentially providing a conservative estimation of the fatigue limit.[137]

TABLE 2 A summary of fatigue indicators and specific implementation.

Method	Index	Author(s)	Year	Procedures	Fatigue limit estimation procedure
Direct temperature assessment	Mean temperature increase	La Rosa & Risitano[22,23]	1983& 2000	• The first usage of thermography on fatigue using the stabilized temperature for fatigue limit estimation; the slope of $T_{\text{stabilized}} - \sigma_a$ curve can used for fatigue limit estimation.	Luong–Risitano's method
		Luong[21]	1995	• Estimating the intrinsic dissipation from the mean temperature; • a sharp change in the dissipation-stress amplitude curve can be related to the fatigue limit.	
		Curà et al.[39]	2005	• The method is used as a basic procedure for other methods based on other indices. • Considering a trial fatigue limit and applying some stresses below and above it to find thermal data; finding the intersection of two fitted lines on the thermal data and comparing it with trial one; continuing the process until the trial value and the one from the intersection of thermal data are almost the same; at the end, updated trial value shows the fatigue limit.	Iterative method
		De Finis et al.[25]	2015	• Filtering out the superficial temperatures. • Modeling a linear relation between $\Delta T_{\text{stabilized}}$ and σ_a; evaluating the residual of $\Delta T_{\text{stabilized}}$; The first statistically significant value of temperature residuals was used to estimate the fatigue limit.	Threshold method

TABLE 2 (Continued)

Method	Index	Author(s)	Year	Procedures	Fatigue limit estimation procedure
	Initial slope of the temperature	Khonsari and colleagues[41,42,49]	2012	• A sharp change in the initial temperature rise slope and stress amplitude ($R_\theta - \sigma_a$) curve is used for fatigue limit estimation.	Luong–Risitano's method
Loss of adiabaticity within the thermoelastic stress analysis framework	Thermoelastic phase analysis	Palumbo & Galietti[47]	2017	• Observing the phase change of the temperature signal; • a sharp point in the $\Delta\varphi - \sigma_a$ curve shows the fatigue limit.	Luong–Risitano's method
	First amplitude harmonic	Krapez et al.[30]	2000	• Using the loss of linearity of the trend of the first harmonic of thermoelastic signal with stress amplitude used to estimate the fatigue limit.	/
		De Finis et al.[26]	2019	• Using the first amplitude and phase shift of the thermal signal; • The sharp change in the slope of either of them with stress amplitude is used for fatigue limit estimation.	Threshold-like method
Energy-based approaches	Second amplitude harmonics (SAH)	Shiozawa et al.[32]	2016	• Assessing the accurate dissipated energy (q); • finding a sharp change in $q - \sigma_a$ curve as a fatigue limit.	Luong–Risitano's method
		De Finis et al.[72]	2021	• finding a relationship between the heat dissipated rate and mechanical energy rate; • Estimating the fatigue limit with the trend SAH and plastic work.	/
	Specific Heat loss	Meneghetti[43]	2007	• Finding the heat dissipation based on the cooling rate; • Drawing dissipated energy per cycle—σ_a curve to estimate the fatigue limit.	Luong–Risitano's method
Thermoelastic point inversion or minimum		Risitano and Risitano[52]	2013	• Inspiring from temperature gradient due	

(Continues)

TABLE 2 (Continued)

Method	Index	Author(s)	Year	Procedures	Fatigue limit estimation procedure
temperature in a tensile test				to the advent of the plastic zone in a tensile test; • adding a temperature curve to the typical stress–strain curve; • Finding a point in the curve shows the beginning of the nonlinearity which is associated with the fatigue limit.	Thermoelastic point inversion method

TABLE 3 The capability of different indices to different factors.

		Parameters/indices*					
Item/factor #	Description of the item	1	2	3	4	5	6
1	Sensitivity to the heat diffusion effect	x	x				x
2	Sensitivity to the microstructures, that is, ductility or brittleness	x	x		x	x	x
3	Sensitivity to the environmental condition	x	x	x			

*Indices:

TABLE 4 Comparison fatigue limits obtained from each method with the traditional one.

Material	Method for fatigue limit prediction	Fatigue limit (mean value)	Difference (%)
XC55 steel[22]	Staircase	399	-
	Luong–Risitano	375	6
Fe 510 steel[39]	Staircase	203	-
	Iterative method	199	1.97
17–4 PH Steel[25]	Staircase	212.1	-
	Threshold method	201.7	4.9
Fe360 steel[52]	Staircase	43.5	-
	Thermoelastic point inversion	44	1.15

It should be noted that the results are taken from the publications where each method was proposed for the first time. Furthermore, it is important to emphasize that the predicted values from each method were based on a single test or specimen, which is not adequate for a precise comparison with the staircase method. When only one specimen is tested, the standard deviation theoretically approaches 0; thus, thermal methods do not estimate the scatter in the anticipated fatigue limit, in contrast to the staircase method. However, a useful comparison can be suggested by checking the difference between the fatigue limit estimated via thermographic technique and the fatigue limit determined with the staircase procedure for a 50% survival probability. Another suggestion can be involving more samples in thermographic methods.

After comparing the accuracy, as listed in Table 5, a concise overview of different features that significantly affect the effectiveness (the first row in Table 5) and applicability (rows 2, 3, and 4 in Table 5) of the

TABLE 5 Summary of different features of the fatigue limit prediction methods.

Features				Fatigue limit estimation procedure			
				(I) Luong–Risitano	(II) Iterative method	(III) Threshold method	(IV) Thermoelastic point inversion
1	Factors affecting the accuracy of fatigue limit estimations	Loading block definition	"Step dimension" between two loading blocks	YES	YES	YES	-
			Minimum number of loading blocks	More than 10[22]	More than 10[39]	Below 10 25	-
			Stress of the first loading block	Not specified	Not specified	σ_{max} =30% UTS	-
		Number of specimens required		Dependence on the definition of loading blocks	Dependence on the definition of loading blocks	Dependence on the definitions of loading blocks	Dependence on the loading rate in the tensile test
2	Possibility to be done automatically			NO	YES	NO	NO
3	Applicability to more than one thermal index			YES	-	YES	NO
4	Analytical expression to evaluate the uncertainty			NO	NO	NO	NO

thermographic method in fatigue limit prediction is proposed. These features can be helpful to investigate uncertainties in fatigue limit estimation procedures.

From Table 5, the first considered feature is the effect of the loading block definition and the number of samples on the accuracy of the predicted fatigue limit.

On the one hand, it is important to recognize that the definition of loading blocks is a highly influential factor, as inappropriate settings could lead to underestimation/overestimation of the fatigue limit. As shown in Table 5, the step dimension including the load increment from one step to another and the number of cycles for each block (see Figure 25), is one of the main parts of the loading blocks definition that should be considered for methods (I)–(III). Furthermore, the number of loading blocks is another part of this procedure. According to the literature,[22,25,39] method (III) can make predictions using fewer than 10 loading blocks, unlike methods (I) and (II) which require more. Thus, it can be concluded that method (III) is more time-efficient when compared to methods (I) and (II). Finally, the last part of the loading block definition is the stress level of the first block. Unlike methods (I) and (II), the load of the initial block is clearly mentioned for method (III), which is approximately 30% of the ultimate tensile stress (in terms of maximum stress).[25]

On the other hand, another factor highlighted in Table 5 is the number of samples required by each method to estimate the fatigue limit with the desired accuracy. As can be seen from Table 5, this factor is basically dependent on the loading block definition. In a different way, the number of samples in method (IV) also relies on the loading rate during the tensile test.

Certainly, the least number of samples required for each method affects significantly both the time and cost of the test. In methods (I)–(III), samples should be under the cyclic loading up to the stabilized temperature for each loading block, theoretically necessitating only one sample to estimate the fatigue limit, since the loading is removed before any damage occurs.[22,25,124] However, uncertainties related to the environmental conditions, material microstructure, geometry, and so forth, introduce statistical variations in results from one sample to another.[124] Accounting for this variability while keeping the test fast, at least three samples are typically recommended.[22,124] Therefore, the estimation of the fatigue limit with only one specimen is useful only for exploratory purposes.

In method (II), it can be expected that having an insufficient number of points in $T-\sigma_a$ could make it challenging to fit straight lines into the thermal data.[39] Thus, it can be concluded that more thermal data seems to be needed in this method than in (I) and (III). Consequently, obtaining additional thermal data may necessitate more testing time and of course, more samples (the more thermal points, the higher the possibility of damage initiation) might be required.

In method (III), the identification of the relation between the temperature rise and stress amplitude, as well as finding the threshold value, can be accomplished during the initial loading steps. Once the residual exceeds the threshold value, the fatigue limit can be estimated without the need for further loading. Theoretically, this method has the potential to introduce a new generation of non-destructive fatigue testing, suggesting that method (III) can offer faster fatigue limit predictions compared to methods (I) and (II).

According to Risitano and Risitano,[52] the thermoelastic point inversion method is faster than the methods with cyclic loading, methods (I)–(III). However, it is important to note that this method relies on the loading rate of the tensile test, as indicated in Table 5. To effectively apply this method, it is necessary to perform some trial tests at different stress rates to observe a sharp and clear slope change in the temperature trend. Following this, additional tests should be conducted using the loading rate identified in the previous step, considering possible scatter as explained by Foti et al.[19]

The second feature in Table 5 is the ability to automatically conduct a thermographic method. Out of the four mentioned methods, only method (II) has this capability.

From the third feature, method (IV) stands out as it can exclusively utilize the mean temperature, unlike methods (I) and (III). It should be noted that the Iterative method (method [II]) has not been tested with indices other than the mean temperature. However, theoretically, it might be possible to apply this method to other indices, particularly indices 5 and 6 in Section 6.1.

Finally, as shown in the last row of Table 5, it is important to highlight that all considered methods share a common limitation: None of them provide an estimation for the uncertainty associated with the assessed fatigue limit.

6.3 | Fatigue limit prediction in components

In this section, after discussing different aspects of thermal fatigue indicators and thermographic techniques, it is important to delve into the challenges associated with assessing the fatigue of components using thermographic techniques.

One of the issues with the thermographic methods is their application to out-of-laboratory case studies, such as the in-situ inspections of components under operating loads. From a practical standpoint, the in-situ inspection requires having sufficient space to set up the equipment (IR camera, computer, etc.) with high spatial resolution and the possibility to increase the emissivity of the component by applying the black coating. Of course, it is essential to have prior knowledge of the critical regions of the components and the loading condition.

Applying laboratory techniques to real-world applications introduces an additional challenge, particularly concerning component geometry. In thicker components, the presence of internal heat sources can create a minimal thermal footprint on the surface, making it challenging to detect without conducting specific postprocessing analyses to differentiate the heat source's subtle signal from background noise. Without such analyses, identifying the most critical areas in components with complex shapes can be quite difficult due to heat dissipation occurring at various points. In such cases, the finite element model can be suggested as it provides valuable support in pinpointing the most stressed regions.

In addition to the challenges mentioned earlier, the stress history and the actual stress state are often unknown in advance, especially for components under operational loads. Therefore, it is not a straightforward task to establish a direct connection between the measured thermal data and the state of stress state as well as the remaining life.

Considering the analyses conducted in previous sections, it becomes evident that, before applying a certain thermographic method to a specific component made of a specific material, it is crucial to fine-tune all the procedures in the laboratory.

Indeed, taking into account the issues mentioned earlier, determining the fatigue limit of metals at the component level poses a significant challenge. This is highlighted by the limited number of studies dedicated to this topic on components, especially when compared to the extensive research conducted on flat and cylindrical samples. To date, only two notable studies can be found in the literature.

The first attempt was undertaken by Luong[28,81] on XC55 steel connecting rods under tension–compression fatigue tests. The study showed that the fatigue limit can be found within a few hours, a significant improvement compared to the several months typically required when using the standard staircase method.[28,81]

In the most recent study by Faria et al,[152] the thermographic method was used for fast prediction of a relatively more complex component, a cast iron crankshaft. The results showed a strong correlation between thermographic findings and the data obtained through the staircase method, particularly for dog bone samples extracted from the crankshaft counterweights.

7 | CONCLUSIONS

This study conducted a comparative review of thermography-based methods and procedures for estimating the fatigue limit. The realm of thermal fatigue assessment was explored with an examination of all thermal indices, including the mean temperature rise, the initial slope of the temperature, the thermoelastic phase, the first amplitude harmonic of temperature, the second amplitude harmonic of temperature and the specific heat loss, employed for either the fatigue limit prediction or the material damage evaluation. Furthermore, all rapid methods, including Loung-Risitano's method, the iterative method, the threshold method, and thermoelastic point inversion in tensile tests, for estimating the fatigue limit were investigated.

On the one hand, the strengths and weaknesses of each thermal index were presented, enabling the selection of the most appropriate one for specific testing conditions. On the other hand, a comparison was made among rapid thermographic methods for estimating the fatigue limit. This comparison considered features like the accuracy and key features affecting their effectiveness, such as how the loading block is defined, and the number of specimens required. Additionally, the applicability of the thermographic methods, including the potential for automation, suitability for multiple thermal indices, and the level of variability in the estimations, were discussed. This analysis helped uncover uncertainties in the estimation of fatigue limits.

Furthermore, challenges in using thermographic techniques for fatigue assessment in real-world scenarios, such as enough space in-situ inspection, prior knowledge of critical regions and loads, geometry complexity, and stress history in the component, were proposed.

In conclusion, it can be stated that

- the thermal indices tied to specific physical processes (thermoelastic effect, intrinsic dissipation, non-adiabatic effects, etc.) are effective parameters for studying the damage from both qualitative and quantitative points of view;
- further exploration of the connection between these processes and the microstructural phenomena related to damage is needed to understand better the meaning of the thermal fatigue limit;
- the harmonic parameters of the temperature signal provide a more robust method for damage assessment than simply using the mean temperature;
- while thermographic methods for estimating the fatigue limit are rapid and promising, additional work is needed to establish a procedure for calculating the uncertainty of the prediction, even with limited samples, to align with standard test methods;
- the application of thermographic methods and procedures in real-world applications is an ongoing topic that requires more effort.

NOMENCLATURE

A_1, A_2, a, b	material constants
C_p	specific heat [J/kg K]
E	module of elasticity [Pa]
$\dot{E}_d$	portion of supplied mechanical power that converts into heating [W/m^3]
$\dot{E}_{d_{2w}}$	second amplitude harmonic of heat dissipated [W/m^3]
$\dot{E}_{rev}$	power of reversible energy variations [W/m^3]
$\dot{E}_s$	rate of internal energy that does not convert into heating [W/m^3]
F	cyclic load in fatigue test [N]
f	frequency of loading [Hz]
k	thermoelastic coefficient [m^3/J]
N	number of cycles
N_f	number of cycles to failure
$\dot{Q}$	heat rate exchanged with the environment [W/m^3]
q	heat flux [W/m^2]
R	stress ratio
R_i, R_θ	slope of temperature at the beginning of the temperature trend
R_r	relative slope of temperature at the beginning of the temperature trend
$\dot{s}_e$	entropy flow [W/m^3°C]
T	Temperature [°C]
T_0	reference temperature [°C]
$T_{1\omega}$, T_1	first amplitude harmonic of temperature [°C]
T_{2w}, T_2	second amplitude harmonic of temperature [°C]
T_a	amplitude of the temperature [°C]
T_d	dissipative temperature [°C]
T_E	thermoelastic temperature [°C]
$T_{elastic}$	temperature due to elastic deformation [°C]
T_{max_r}	residual temperature [°C]
$T_{plastic}$	temperature due to elastic deformation [°C]
$T_{stabilized}$	stabilized temperature rise [°C]

T_{the}	thermoelastic amplitude of the temperature [$^{\circ}C$]
t_f	time up to the fatigue failure [s]
$\dot{U}$	internal energy rate [W/m^3]
$\dot{W}$	mechanical energy rate [W/m^3]
W_p	plastic energy [J]
$\dot{W}_{2w}$	second amplitude harmonic of mechanical energy [W/m^3]
α	linear thermal expansion coefficient [$1/^{\circ}C$]
γ_f	fatigue fracture entropy [$W/m^{3\circ}C$]
Δs	first invariant change of the stress tensor [Pa]
ΔT	temperature rise [$^{\circ}C$]
ε	strain
θ	slope of temperature at the end of temperature trend
θ_E	phase lag due to thermal diffusion
θ_D	phase lag due to thermal diffusion
ρ	density [kg/m^3]
Σ_0	cyclic load in fatigue test [N]
σ	stress [Pa]
σ_a	stress amplitude [Pa]
σ_0, σ_y	yield stress [Pa]
σ_i	stress level [Pa]
σ_c	fatigue limit [Pa]
φ	phase angle between temperature and loading signal
φ_1	Phase of the first Fourier component of temperature
φ_2	phase of the second Fourier component of temperature
Ψ	damping capacity
ω	angular frequency [Hz]

AUTHOR CONTRIBUTIONS

Each person who meets the established criteria for authorship is acknowledged as an author, and all authors have adequately engaged in this study to accept public accountability for its content. This encompassing involvement includes active participation in the conceptions, planning, writing, and revision of the manuscript.

ACKNOWLEDGMENTS

The activities have been financed by the European Union—NextGenerationEU (National Sustainable Mobility Center CN00000023, Italian Ministry of University and Research Decree n. 1033 - 17/06/2022, Spoke 11 - Innovative Materials & Lightweighting). The opinions expressed are those of the authors only and should not be considered as representative of the European Union or the European Commission's official position. Neither the European Union nor the European Commission can be held responsible for them.

CONFLICT OF INTEREST STATEMENT

The authors declare no conflict of interest.

DATA AVAILABILITY STATEMENT

The data that support the findings of this study are available from the corresponding author upon reasonable request.

REFERENCES

1. Shepard SM. *Advances in Pulsed Thermography. Paper Presented at: Advances in pulsed Thermography*. Proc. SPIE—The International Society for Optical Engineering, Thermosense XXVIII2001.
2. Rajic N. Principal component thermography. In: *Airframes and Engines Division Aeronautical and Maritime Research Laboratory, DSTO-TR-1298*; 2002.
3. Ibarra-Castanedo C, Avdelidis NP, Maldague XP. *Quantitative Pulsed Phase Thermography Applied to Steel Plates*. International Society for Optics and Photonics2005.
4. Balageas DL, Roche J-M, Leroy F-H, Liu W-M, Gorbach AM. The thermographic signal reconstruction method: a powerful tool for the enhancement of transient thermographic images. *Biocybernet Biomed Eng*. 2015;35(1):1-9.
5. Angioni SL, Ciampa F, Pinto F, Scarselli G, Almond DP, Meo M. An analytical model for defect depth estimation using pulsed thermography. *Exp Mech*. 2016;56(6):1111-1122.
6. D'Accardi E, Palumbo D, Galietti U. Experimental procedure to assess depth and size of defects with pulsed thermography. *J Nondestructive Eval*. 2022;41(2):41.
7. Pitarresi G, Cappello R, Capraro A, Pinto V, Badagliacco D, Valenza A. *Frequency modulated thermography-NDT of polymer composites by means of human-controlled heat modulation*. Paper presented at European Workshop on Structural Health Monitoring; 2023.
8. D'Accardi E, Krankenhagen R, Ulbricht A, et al. Capability to detect and localize typical defects of laser powder bed fusion (L-PBF) process: an experimental investigation with different non-destructive techniques. *Progr Addit Manuf*. 2022;7(6):1239-1256.
9. Dell'Avvocato G, Gohlke D, Palumbo D, Krankenhagen R, Galietti U. *Quantitative evaluation of the welded area in resistance projection welded (RPW) thin joints by pulsed laser thermography*. Vol. 12109. SPIE; 2022.
10. Montinaro N, Cerniglia D, Pitarresi G. Evaluation of vertical fatigue cracks by means of flying laser thermography. *J Nondestructive Eval*. 2019;38(2):48.
11. Jiménez-Fortunato I, Bull DJ, Thomsen OT, Dulieu-Barton JM. Quantitative microbolometer-based thermoelastic stress analysis. *Opt Lasers Eng*. 2023;160:107276.
12. Dulieu-Barton J. *Thermoelastic Stress Analysis. Optical Methods for Solid Mechanics*. John Wiley & Sons; 2012:345-366.
13. Harwood N, Cummings WM. *Thermoelastic Stress Analysis*. Adam Hilger; 1991.
14. Palumbo D, De Finis R, Galietti U. Thermoelastic stress analysis as a method for the quantitative non-destructive evaluation of bonded CFRP T-joints. *NDT & E Int*. 2021;124:102526.

15. Wang WJ, Dulieu-Barton JM, Li Q. Assessment of non-adiabatic behaviour in thermoelastic stress analysis of small scale components. *Exp Mech*. 2010;50(4):449-461.
16. Stanley P. Beginnings and early development of thermoelastic stress analysis. *Strain*. 2008;44(4):285-297.
17. Feltner CE, Morrow JD. Microplastic strain hysteresis energy as a criterion for fatigue fracture. *J Basic Eng*. 1961;83(1): 15-22.
18. Chrysochoos A, Louche H. An infrared image processing to analyse the calorific effects accompanying strain localisation. *Int J Eng Sci*. 2000;38(16):1759-1788.
19. Foti P, Santonocito D, Ferro P, Risitano G, Berto F. Determination of fatigue limit by static thermographic method and classic thermographic method on notched specimens. *Proc Struct Integr*. 2020;26:166-174.
20. Amiri M, Khonsari MM. Nondestructive estimation of remaining fatigue life: thermography technique. *J Failure Anal Prevent*. 2012;12(6):683-688.
21. Luong MP. Infrared thermographic scanning of fatigue in metals. *Nuclear Eng Des*. 1995;158(2):363-376.
22. La Rosa G, Risitano A. Thermographic methodology for rapid determination of the fatigue limit of materials and mechanical components. *Int J Fatigue*. 2000;22(1):65-73.
23. Geraci A, Rosa GL, Risitano A. *L'infrarosso termico nelle applicazioni meccaniche. CRES Symp. CRES Symposium*; 1983.
24. Catalbiano T, Geraci A, Orlando M. Analisi tramite infrarosso termico di provini sollecitati a fatica. *Il Progettista Industriale*. 1984;12:88-99.
25. De Finis R, Palumbo D, Ancona F, Galietti U. Fatigue limit evaluation of various martensitic stainless steels with new robust thermographic data analysis. *Int J Fatigue*. 2015;74: 88-96.
26. De Finis R, Palumbo D, Galietti U. A multianalysis thermography-based approach for fatigue and damage investigations of ASTM A182 F6NM steel at two stress ratios. *Fatigue Fract Eng Mater Struct*. 2019;42(1):267-283.
27. Rosa GL, Risitano A. *Application of a New Methodology to Determine the Fatigue Limit Using Thermal Infrared Techniques*. 17th Symposium on Experimental Mechanics; 1996.
28. Luong MP. *Infrared Thermography of Fatigue in Metals*. SPIE; 1682, 1992.
29. Geraci A, Rosa GL, Risitano A. *Influence of Frequency and Cumulative Damage on the Determination of Fatigue Limit of Materials Using the Thermal Infrared Methodology*. 15th Symposium on Experimental Mechanics of Solids; 1992.
30. Krapez JC, Pacou D, Gardette G. Lock-in thermography and fatigue limit of metals. *Quantitative InfraRed Thermography*. 2000;277–282.
31. Bremont P, Potet PD. *Démodulation Synchrone des Images Thermiques. Application à L'analyse Expérimentale des Structures. Journée de la Société Française des Thermiciens, Thermographie Quantitative*. 1994.
32. Shiozawa D, Inagawa T, Washio T, Sakagami T. Fatigue limit estimation of stainless steels with new dissipated energy data analysis. *Proc Struct Integr*. 2016;2:2091-2096.
33. Boulanger T, Chrysochoos A, Mabru C, Galtier A. Calorimetric analysis of dissipative and thermoelastic effects associated with the fatigue behavior of steels. *Int J Fatigue*. 2004;26(3): 221-229.
34. Rigon D, Berto F, Meneghetti G. Estimating the multiaxial fatigue behaviour of C45 steel specimens by using the energy dissipation. *Int J Fatigue*. 2021;151:106381.
35. Munier R, Doudard C, Calloch S, Weber B. Determination of high cycle fatigue properties of a wide range of steel sheet grades from self-heating measurements. *Int J Fatigue*. 2014;63: 46-61.
36. Gough J. A description of a property of Caoutchouc, or India rubber; with some reflections on the cause of the elasticity of this substance. *Memoirs Literary Philos Soc Manchester*. 1805; 1:288-295.
37. Ranc N, Wagner D, Paris PC. Study of thermal effects associated with crack propagation during very high cycle fatigue tests. *Acta Mater*. 2008;56(15):4012-4021.
38. Plekhov OA, Naimark OB. Theoretical and experimental study of energy dissipation in the course of strain localization in iron. *J Appl Mech Tech Phys*. 2009;50(1): 127-136.
39. Curà F, Curti G, Sesana R. A new iteration method for the thermographic determination of fatigue limit in steels. *Int J Fatigue*. 2005;27(4):453-459.
40. Colombo C, Vergani L. Thermographic applications for the rapid estimation of fatigue limit. *Proc Struct Integr*. 2019;24: 658-666.
41. Amiri M, Khonsari MM. Life prediction of metals undergoing fatigue load based on temperature evolution. *Mater Sci Eng A*. 2010;527(6):1555-1559.
42. Amiri M, Khonsari MM. Rapid determination of fatigue failure based on temperature evolution: fully reversed bending load. *Int J Fatigue*. 2010;32(2):382-389.
43. Meneghetti G. Analysis of the fatigue strength of a stainless steel based on the energy dissipation. *Int J Fatigue*. 2007;29(1): 81-94.
44. Enke NF, Sandor BI. Cyclic plasticity analysis by differential infrared thermography. In: *Proceedings of the VII International Congress on Experimental Mechanics*; 1988.
45. Krapez J-C, Pacou D, Bertin C. Application of lock-in thermography to rapid evaluation of fatigue limit in metals. In: *Workshop on Advanced Infrared Technology and Applications*; 1999.
46. Pitarresi G, Cappello R. Evaluation of crack-closure by second harmonic thermoelastic stress analysis. *Int J Fatigue*. 2022; 164:107116.
47. Palumbo D, Galietti U. Thermoelastic phase analysis (TPA): a new method for fatigue behaviour analysis of steels. *Fatigue Fract Eng Mater Struct*. 2017;40(4):523-534.
48. De Finis R. *Application of Thermal Methods Based on Infrared Thermography for the Mechanical Characterisation of Materials* [doctoral thesis]. Polytechnic University of Bari; 2017.
49. Mehdizadeh M, Khonsari MM. On the application of fracture fatigue entropy to variable frequency and loading amplitude. *Theoret Appl Fracture Mech*. 2018;98:30-37.
50. Galietti U, Palumbo D, Finis RD, Ancona F. *Fatigue Limit Evaluation of Martensitic Steels with Thermal Methods. Conference QIRT*. Bordeaux; 2014.

51. Risitano A, Fargione G, Guglielmino E. Definition of the linearity loss of the surface temperature in static tensile tests. *Frattura Ed Integrità Strutturale*. 2014;8(30):201-210.
52. Risitano A, Risitano G. Determining fatigue limits with thermal analysis of static traction tests. *Fatigue Fract Eng Mater Struct*. 2013;36(7):631-639.
53. Rosner H, Sathish S, Meyendorf N. Thermographic characterisation of fatigue. In: Thompson D, Chimenti D, eds. *Review of progress in QNDE*. Vol.20; 2001.
54. Suresh S. *Fatigue of Materials*. Vol. 8. Cambridge solid state science series; 1992.
55. Pedersen MM. *Introduction to Metal Fatigue*. Aarhus University; 2018.
56. Stephens RI, Fatemi A, Stephens RR, Fuchs HO. *Metal Fatigue in Engineering*. 2nd ed. Wiley; 2000.
57. Jordan EH. Notch-root plastic response by temperature measurement. *Exp Mech*. 1985;25(1):24-31.
58. Nourian-Avval A, Khonsari MM. Rapid prediction of fatigue life based on thermodynamic entropy generation. *Int J Fatigue*. 2021;145:106105.
59. Ewing JA, Rosenhain W. Experiments in micro-metallurgy: effects of strain. Preliminary notice. *Proc R Soc London*. 1900; 65(413–422):85-90.
60. Bauschinger J. *Ueber die Veranderungen der Elastizitatsgrenze und der Festigkeit des Eisens und Stahls Durch Strecken, Quetschen, Erwarmen Abkiihlen und Durch Oftmals Wiederholte Belastung*. Mitt: Mech-Tech Lab, XIII Miinchen; 1986.
61. Audenino AL, Zanetti EM, Calderale PM. Assessment of internal damping in uniaxially stressed metals: exponential and autoregressive methods. *J Dynam Syst Meas Control*. 1998;120(2):177-184.
62. Schijve J. *Fatigue of Structures and Materials*. Springer; 2009.
63. Murakami Y. *Metal Fatigue: Effects of Small Defects and Nonmetallic Inclusions*. 2nd ed. Academic Press; 2019.
64. Ewing JA, Humfrey JCW. VI. The fracture of metals under repeated alternations of stress. *Philos Trans R Soc London Ser A*. 1903;200(321–330):241-250.
65. Sakai T, Nakagawa A, Oguma N, et al. A review on fatigue fracture modes of structural metallic materials in very high cycle regime. *Int J Fatigue*. 2016;93:339-351.
66. Srivatsan S, Sudarshan TS. Mechanisms of fatigue crack initiation in metals: role of aqueous environments. *J Mater Sci*. 1988;23(5):1521-1533.
67. Chrysochoos A, Huon V, Jourdan F, Muracciole J-M, Peyroux R, Wattrisse B. Use of full-field digital image correlation and infrared thermography measurements for the thermomechanical analysis of material behaviour. *Strain*. 2010; 46(1):117-130.
68. Mughrabi H. Dislocations in fatigue. In: *Dislocations and Properties of Real Materials*. Institute of Metals; 1985.
69. Scott-Emuakpor O, George T, Cross C, Shen M-HH. Hysteresis-loop representation for strain energy calculation and fatigue assessment. *J Strain Anal Eng Des*. 2010;45(4):275-282.
70. Fancher DR. *Stress-strain hysteresis loops and rheological epicycles*. The University of Arizona; 1943.
71. Lazan BJ. Effect of damping constants and stress distribution on the resonance response of members. *J Appl Mech*. 1953; 20(2):201-209.
72. De Finis R, Palumbo D, Galietti U. On the relationship between mechanical energy rate and heat dissipated rate during fatigue for a C45 steel depending on stress ratio. *Fatigue Fract Eng Mater Struct*. 2021;44(10):2781-2799.
73. Meneghetti G, Ricotta M. Estimating the intrinsic dissipation using the second harmonic of the temperature signal in tension–compression fatigue. Part II: experiments. *Fatigue Fract Eng Mater Struct*. 2021;44(8):2153-2167.
74. Colombo C, Sansone M, Patriarca L, Vergani L. Rapid estimation of fatigue limit for C45 steel by thermography and digital image correlation. *J Strain Anal Eng Des*. 2021;56(7):478-491.
75. Chaboche JL, Nouailhas D, Pacou D, Paulmier P. Modeling of the cylic response and ratchetting effects on inconel-718 alloy. *Eur J Mech A-Solids*. 1991;10:101-121.
76. Lachowicz CT. Calculation of the elastic–plastic strain energy density under cyclic and random loading. *Int J Fatigue*. 2001; 23(7):643-652.
77. Colombo C, Fumagalli G, Bolzoni F, Gobbi G, Vergani L. Fatigue behavior of hydrogen pre-charged low alloy Cr–Mo steel. *Int J Fatigue*. 2016;83:2-9.
78. Crupi V. An unifying approach to assess the structural strength. *Int J Fatigue*. 2008;30(7):1150-1159.
79. Connesson N, Maquin F, Pierron F. Experimental energy balance during the first cycles of cyclically loaded specimens under the conventional yield stress. *Exp Mech*. 2011;51(1): 23-44.
80. Maquin F, Pierron F. Heat dissipation measurements in low stress cyclic loading of metallic materials: from internal friction to micro-plasticity. *Mech Mater*. 2009;41(8):928-942.
81. Luong MP. Fatigue limit evaluation of metals using an infrared thermographic technique. *Mech Mater*. 1998;28(1-4): 155-163.
82. Naderi M, Khonsari MM. An experimental approach to low-cycle fatigue damage based on thermodynamic entropy. *Int J Solids Struct*. 2010;47(6):875-880.
83. Mareau C. *Micromechanical Modeling of Self-Heating and Microplasticity in Steels Under Cyclic Loading*. Arts et Métiers ParisTech; 2007.
84. Doudard C, Calloch S, Cugy P, Galtier A, Hild F. A probabilistic two-scale model for high-cycle fatigue life predictions. *Fatigue Fract Eng Mater Struct*. 2005;28(3):279-288.
85. Stromeyer CE, Dalby WE. The determination of fatigue limits under alternating stress conditions. *Proc R Soc London Ser A*. 1914;90(620):411-425.
86. Curti G, Rosa GL, Orlando M, Risitano A. *Analisi Tramite Infrarosso Termico Della Temperatura Limite in Prove di Fatica*. XIV Convegno Nazionale AIAS; 1986.
87. Crupi V, Guglielmino E, Maestro M, Marinò A. Fatigue analysis of butt welded AH36 steel joints: thermographic method and design S–N curve. *Mar Struct*. 2009;22(3):373-386.
88. Wang XG, Crupi V, Guo XL, Zhao YG. Quantitative thermographic methodology for fatigue assessment and stress measurement. *Int J Fatigue*. 2010;32(12):1970-1976.
89. Fargione G, Geraci A, La Rosa G, Risitano A. Rapid determination of the fatigue curve by the thermographic method. *Int J Fatigue*. 2002;24(1):11-19.
90. Wang XG, Crupi V, Guo XL, Guglielmino E. A thermography-based approach for structural analysis and fatigue evaluation.

Proc Inst Mech Eng Part C: J Mech Eng Sci. 2011;226(5):1173-1185.

91. Wang XG, Crupi V, Jiang C, Guglielmino E. Quantitative thermographic methodology for fatigue life assessment in a multiscale energy dissipation framework. *Int J Fatigue*. 2015;81:249-256.
92. Feng E, Wang X, Jiang C, Crupi V. Quantitative thermographic method for fatigue life prediction under variable amplitude loading. *Fatigue Fract Eng Mater Struct*. 2022;45(4):1199-1212.
93. Aeran A, Vantadori S, Carpinteri A, Siriwardane SC, Scorza D. Novel non-linear relationship to evaluate the critical plane orientation. *Int J Fatigue*. 2019;124:537-543.
94. Huang Y, Li SX, Lin SE, Shih CN. Using the method of infrared sensing for monitoring fatigue process of metals. *Mater Eval*. 1984;42(8):1020-1024.
95. Botny R, Kaleta J. A method for determining the heat energy of the fatigue process in metals under uniaxial stress: part 1. Determination of the amount of heat liberated from a fatigue-tested specimen. *Int J Fatigue*. 1986;8(1):29-33.
96. Meyendorf NG, Rösner H, Kramb V, Sathish S. Thermoacoustic fatigue characterization. *Ultrasonics*. 2002;40(1–8):427-434.
97. Liakat M, Khonsari MM. An experimental approach to estimate damage and remaining life of metals under uniaxial fatigue loading. *Mater Des*. 2014;57:289-297.
98. Liakat M, Khonsari MM. Rapid estimation of fatigue entropy and toughness in metals. *Mater des (1980–2015)*. 2014;62:149-157.
99. Weber W. Ueber die specifische wärme fester körper, insbesondere der metalle. *Ann Phys*. 1830;96(10):177-213.
100. Thomson W II. On the dynamical theory of heat, with numerical results deduced from Mr. Joule's equivalent of a thermal unit, and M. Regnault's observations on steam. *London Edinburgh Dublin Philos Mag J Sci*. 1852;4(22):8-21.
101. Harwood N, Cummings WM. *Thermoelastic stress analysis*. National Engineering Laboratory, Adam Hilger; 1991.
102. Wong AK, Sparrow JG, Dunn SA. On the revised theory of the thermoelastic effect. *J Phys Chem Solid*. 1988;49(4):395-400.
103. Pitarresi G, Patterson EA. A review of the general theory of thermoelastic stress analysis. *J Strain Anal Eng Des*. 2003;38(5):405-417.
104. Wong AK, Jones R, Sparrow JG. Thermoelastic constant or thermoelastic parameter? *J Phys Chem Solid*. 1987;48(8):749-753.
105. Wong AK, Dunn SA, Sparrow JG. Residual stress measurement by means of the thermoelastic effect. *Nature*. 1988;332(6165):613-615.
106. Sakagami T, Kubo S, Tamura E, Nishimura T. *Identification of Plastic-Zone Based on Double Frequency Lock-in Thermographic Temperature Measurement*. 2013.
107. Galietti U, Palumbo D, Finis RD, Ancona F. *Fatigue Damage Evaluation with New Thermal Methods*. 3rd International Workshop on Advanced Infrared Technology and Applications; 2013.
108. Dulieu-Barton JM. Introduction to thermoelastic stress analysis. *Strain*. 1999;35(2):35-39.
109. Offermann S, Beaudoin JL, Bissieux C, Frick H. Thermoelastic stress analysis under nonadiabatic conditions. *Exp Mech*. 1997;37(4):409-413.
110. Cappello R, Meneghetti G, Ricotta M, Pitarresi G. On the correlation of temperature harmonic content with energy dissipation in C45 steel samples under fatigue loading. *Mech Mater*. 2022;168:104271.
111. De Finis R, Palumbo D, Galietti U. Mechanical behaviour of stainless steels under dynamic loading: an investigation with thermal methods. *J Imaging*. 2016;2(4):32.
112. Jasper TM. LXVII. The value of the energy relation in the testing of ferrous metals at varying ranges of stress and at intermediate and high temperatures. *London Edinburgh Dublin Philos Mag J Sci*. 1923;46(274):609-627.
113. Hanstock RF. Damping capacity, strain hardening and fatigue. *Proc Phys Soc*. 1947;59(2):275-287.
114. Liao D, Zhu S-P, Gao J-W, Correia J, Calçada R, Lesiuk G. Generalized strain energy density-based fatigue indicator parameter. *Int J Mech Sci*. 2023;254:108427.
115. Zhu S-P, Liu Y, Liu Q, Yu Z-Y. Strain energy gradient-based LCF life prediction of turbine discs using critical distance concept. *Int J Fatigue*. 2018;113:33-42.
116. Liao D, Zhu S-P. Energy field intensity approach for notch fatigue analysis. *Int J Fatigue*. 2019;127:190-202.
117. Zhu S-P, Yu Z-Y, Liu Q, Ince A. Strain energy-based multiaxial fatigue life prediction under normal/shear stress interaction. *Int J Damage Mech*. 2019;28(5):708-739.
118. Shiozawa D, Inagawa T, Washio T, Sakagami T. Accuracy improvement in dissipated energy measurement by using phase information. *Meas Sci Technol*. 2017;28(4):044004.
119. Finis RD, Palumbo D, Pirinu A, et al. Fatigue behaviour assessment of C45 steel by means of energy-based methods. *IOP Conf Ser: Mater Sci Eng*. 2021;1038:012015.
120. Meneghetti G, Ricotta M. Estimating the intrinsic dissipation using the second harmonic of the temperature signal in tension–compression fatigue: part I. *Theory Fatigue Fracture Eng Mater Struct*. 2021;44(8):2168-2185.
121. Meneghetti G, Ricotta M. Evaluating the heat energy dissipated in a small volume surrounding the tip of a fatigue crack. *Int J Fatigue*. 2016;92:605-615.
122. Meneghetti G, Ricotta M. The heat energy dissipated in the material structural volume to correlate the fatigue crack growth rate in stainless steel specimens. *Int J Fatigue*. 2018;115:107-119.
123. Meneghetti G, Ricotta M. The use of the specific heat loss to analyse the low- and high-cycle fatigue behaviour of plain and notched specimens made of a stainless steel. *Eng Fracture Mech*. 2012;81:2-16.
124. Ricotta M, Meneghetti G, Atzori B, Risitano G, Risitano A. Comparison of experimental thermal methods for the fatigue limit evaluation of a stainless steel. *Metals*. 2019;9(6):677.
125. Rigon D, Ricotta M, Meneghetti G. An analysis of the specific heat loss at the tip of severely notched stainless steel specimens to correlate the fatigue strength. *Theoret Appl Fracture Mech*. 2017;92:240-251.
126. Skibicki D, Lipski A, Pejkowski Ł. Evaluation of plastic strain work and multiaxial fatigue life in CuZn37 alloy by means of thermography method and energy-based approaches of Ellyin

and Garud. *Fatigue Fract Eng Mater Struct*. 2018;41(12):2541-2556.
127. Naderi M, Amiri M, Khonsari MM. On the thermodynamic entropy of fatigue fracture. *Proc R Soc A: Math Phys Eng Sci*. 2010;466(2114):423-438.
128. Marrow JD. Cyclic plastic strain energy and fatigue of metals. *STM STP*. 1995;378:45-84.
129. Naderi M, Khonsari M. Real-time fatigue life monitoring based on thermodynamic entropy. *Struct Health Monit*. 2011; 10(2):189-197.
130. Jang JY, Khonsari MM. On the evaluation of fracture fatigue entropy. *Theoret Appl Fracture Mech*. 2018;96:351-361.
131. Mehdizadeh M, Khonsari MM. On the role of internal friction in low-and high-cycle fatigue. *Int J Fatigue*. 2018;114:159-166.
132. Liakat M, Khonsari MM. On the anelasticity and fatigue fracture entropy in high-cycle metal fatigue. *Mater des*. 2015;82: 18-27.
133. Haghshenas A, Jang JY, Khonsari MM. On the intrinsic dissipation and fracture fatigue entropy of metals. *Mech Mater*. 2021;155:103734.
134. Guo Q, Guo X, Fan J, Syed R, Wu C. An energy method for rapid evaluation of high-cycle fatigue parameters based on intrinsic dissipation. *Int J Fatigue*. 2015;80:136-144.
135. Bottani CE, Caglioti G. Thermoelastic instabilities in metals. *Phys Scr*. 1982;T1:65-70.
136. Risitano A, Corallo D, Risitano G, Sirugo A. *Determinazione del limite di fatica mediante prove quasistatiche*. Proceedings XXXIX AIAS National Conference; 2010.
137. Risitano G, Guglielmino E, Santonocito D. Rapid energetic approaches for the fatigue limit assessment in a medium carbon steel. *Proc Struct Integr*. 2021;33:748-756.
138. Foti P, Risitano G, Berto F, Santonocito D. Evaluation of the energetic release during tensile tests in notched specimens by means of experimental and numerical techniques. *IOP Conf Ser: Mater Sci Eng*. 2021;1038(1):012038.
139. Risitano G, Santonocito D. Experimental and numerical assessment of the end of the thermoelastic effect during static traction test. *Proc Struct Integr*. 2020;28:1449-1457.
140. Corigliano P, Cucinotta F, Guglielmino E, Risitano G, Santonocito D. Fatigue assessment of a marine structural steel and comparison with thermographic method and static thermographic method. *Fatigue Fract Eng Mater Struct*. 2020; 43(4):734-743.
141. *ASTM E 466, Standard Practice for Conducting Force Controlled Constant Amplitude Axial Fatigue Tests of Metallic Materials*. 1996.
142. De Finis R, Palumbo D, Serio LM, De Filippis LAC, Galietti U. Correlation between thermal behaviour of AA5754-H111 during fatigue loading and fatigue strength at fixed number of cycles. *Dent Mater*. 2018;11(5):719.
143. Deane S, Avdelidis NP, Ibarra-Castanedo C, et al. Comparison of cooled and uncooled IR sensors by means of signal-to-noise ratio for NDT diagnostics of aerospace grade composites. *Sensors (Basel)*. 2020;20(12):3381.
144. Bagavathiappan S, Lahiri BB, Saravanan T, Philip J, Jayakumar T. Infrared thermography for condition monitoring – a review. *Infrared Phys Technol*. 2013;60:35-55.
145. Chrysochoos A, Berthel B, Latourte F, Pagano S, Wattrisse B, Weber B. Local energy approach to steel fatigue. *Strain*. 2008; 44(4):327-334.
146. Morabito AE, Chrysochoos A, Dattoma V, Galietti U. Analysis of heat sources accompanying the fatigue of 2024 T3 aluminium alloys. *Int J Fatigue*. 2007;29(5):977-984.
147. De Finis R, Palumbo D, da Silva MM, Galietti U. Is the temperature plateau of a self-heating test a robust parameter to investigate the fatigue limit of steels with thermography? *Fatigue Fract Eng Mater Struct*. 2018;41(4):917-934.
148. De Finis R, Palumbo D, Ancona F, Galietti U. Fatigue behaviour of stainless steels: a multi-parametric approach. Paper presented at. In: *Residual stress, Thermomechanics & Infrared Imaging, hybrid techniques and inverse problems*. Vol.9; 2017.
149. Kawai R, Yoshikawa T, Kurokawa Y, Irie Y, Inoue H. Rapid evaluation of fatigue limit using infrared thermography: comparison between two methods for quantifying temperature evolution. *Mech Eng J*. 2017;4(5) 17–00009–00017-00009: 17-00009.
150. Lepitre P, Calloch S, Dhondt M, Surand M, Doudard C. Identification of the damage scenarios under cyclic loading of a coated 300M steel by infrared thermography measurements. *Phys Sci Forum*. 2022;4(1):30.
151. Fernández-Canteli A, Castillo E, Argüelles A, Fernández P, Canales M. Checking the fatigue limit from thermographic techniques by means of a probabilistic model of the epsilon–N field. *Int J Fatigue*. 2012;39:109-115.
152. Faria JJR, Fonseca LGA, de Faria AR, et al. Determination of the fatigue behavior of mechanical components through infrared thermography. *Eng Failure Anal*. 2022;134:106018.

How to cite this article: Zaeimi M, De Finis R, Palumbo D, Galietti U. Fatigue limit estimation of metals based on the thermographic methods: A comprehensive review. *Fatigue Fract Eng Mater Struct*. 2024;47(3):611-646. doi:10.1111/ffe.14206